Ore Geology Reviews 89 (2017) 668–682

Contents lists available at ScienceDirect

Ore Geology Reviews

journal homepage: www.elsevier.com/locate/oregeo

Polymetallic (Pb-Zn-Cu-Ag ± Au) vein-type deposits in brittle-ductile transtensional shear zones, Eastern Sierras Pampeanas (Argentina): Age constraints and significance for the Late Paleozoic tectonic evolution and metallogenesis

M. Natalia Maffini [a,*], Klaus Wemmer [b], Stefania Radice [a], Sebastián Oriolo [c], Fernando D'Eramo [a], Jorge Coniglio [a], Manuel Demartis [a], Lucio Pinotti [a]

[a] CONICET – Universidad Nacional de Río Cuarto (UNRC), Departamento de Geología, Ruta Nacional 36 km 601, X5800 Río Cuarto (Córdoba), Argentina
[b] University of Göttingen, Geoscience Centre (GZG), Goldschmidstr. 3, 37077 Göttingen, Germany
[c] CONICET – Universidad de Buenos Aires, Instituto de Geociencias Básicas, Aplicadas y Ambientales de Buenos Aires (IGeBA), Intendente Güiraldes 2160, Facultad de Ciencias Exactas y Naturales, C1428EHA Buenos Aires, Argentina

ARTICLE INFO

Article history:
Received 27 March 2017
Received in revised form 29 June 2017
Accepted 3 July 2017
Available online 5 July 2017

Keywords:
Southern Sierras de Córdoba
Hydrothermal veins
K/Ar fine-fraction dating
Shear zone reactivation
Carboniferous evolution

ABSTRACT

This paper discusses new structural, kinematic and geochronological data from polymetallic (Pb-Zn-Cu-Ag ± Au) vein-type deposits hosted in the metamorphic basement of the southern Sierras de Córdoba. A Carboniferous age was established for the hydrothermal event between ~329 and 315 Ma (Late Mississippian-Early Pennsylvanian) by the K/Ar fine-fraction dating method of sericitic alteration related to metallic ore deposition in the Las Guindas and Oro districts. The obtained ages postdate the spatially associated Devonian magmatism and overlap the A-type Early Carboniferous magmatism defined for the Eastern Sierras Pampeanas. The presence of non-exhumed granitic bodies at shallow depths, possibly related to mineralization, is supported by available geophysical and field evidence.

The strain fabric and 3-D kinematic analyses constitute first kinematic data for the Carboniferous basement of the Southern Sierras Pampeanas demonstrating that mineralization was controlled by NNW- and ENE-trending brittle-ductile transtensional shear zones that overprint the earlier high-strain deformation fabrics of the basement. Transtensional deformation has accommodated large amounts of strike-slip movements and subordinated extensional components. The calculated kinematic axes indicate a coherent kinematic pattern of the mineralized systems in the two studied districts, with a maximum extension direction oriented NNE- to NE and maximum shortening direction oriented WNW- to NW. This deformation regime, active during mineralization, point to a non-compressive setting at the Late Mississippian-Early Pennsylvanian boundary. In line with other regional evidence, we propose a distinctive Carboniferous deformational phase in the Eastern Sierras Pampeanas, dominated by transtension. This period would have occurred after the transition with the Devonian compressional/transpressional orogenic regime.

1. Introduction

The Sierras de Córdoba is the easternmost range system of the Sierras Pampeanas of Argentina (Fig. 1), whose geologic history is intimately related to the geodynamic evolution of the pre-Andean margin of Gondwana. The metallogenic framework of the Sierras de Córdoba includes a wide diversity of mineralization styles and deposits formed during different tectonic events, from the Neoproterozoic to the Cenozoic (de Brodtkorb et al., 2014; Mutti et al., 2007; Mutti et al., 2005). Although the greatest metalliferous potential of this region was historically related to a significant production of W, a relatively large number of polymetallic (following Cox and Singer, 1986) and auriferous vein-type deposits were mined during the 20th century, with production of Ag, Pb, Zn and Au. Likewise, this specialization in base and precious metals is not only confined to the basement of the Sierras de Córdoba, but extends further west and northwest to the provinces of San Luis and La Rioja (Skirrow et al., 2000), and possibly, forms part of a continental-scale Paleozoic gold-rich belt prolonged to the north of Peru (Haeberlin et al., 2003).

* Corresponding author.
E-mail address: nataliamaffini@gmail.com (M.N. Maffini).

http://dx.doi.org/10.1016/j.oregeorev.2017.07.003
0169-1368/

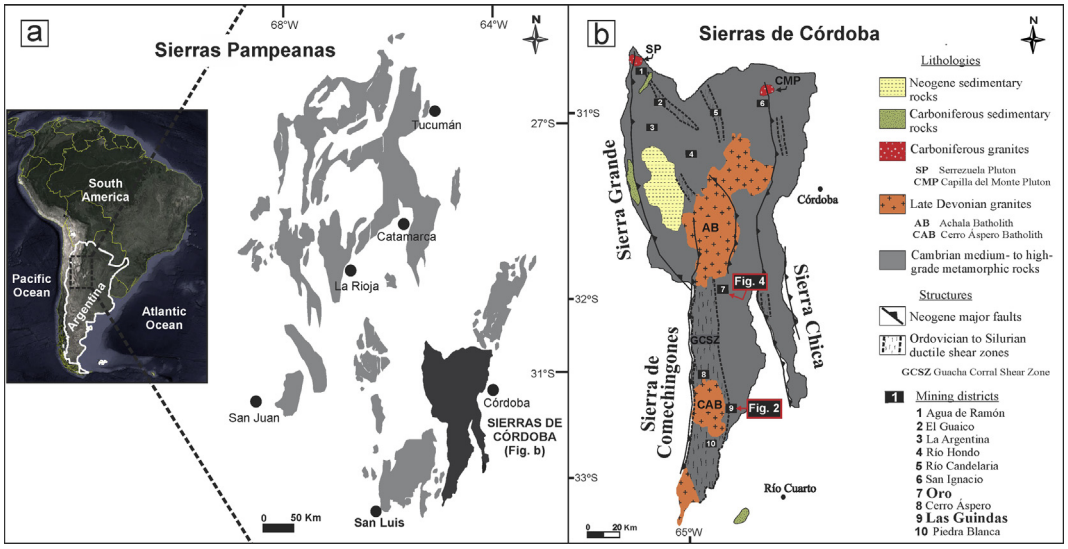

Fig. 1. a) Location of the Sierras de Córdoba in the regional framework of the Sierras Pampeanas of Argentina. b) Simplified geological map of the Sierras de Córdoba including the location of the main mining districts of auriferous, polymetallic and W-bearing vein-type deposits. The two districts studied in this work (Oro and Las Guindas) are indicated.

Until the present, publications focused on the metallogenesis of polymetallic and Au-bearing deposits of the Sierras de Córdoba are restricted to a few districts (Miró, 1999; Mutti et al., 2007; Skirrow et al., 2000; Sureda, 1978) and geochronological constraints on the timing of mineralization are still scarce. With regard to this aspect, the largest amount of age data ($^{40}Ar/^{39}Ar$ dating of sericitic alteration) was reported and compiled by Skirrow et al. (2000), who defined a Devonian metallogenic epoch between ~390 and 360 Ma, temporally and spatially related to a major magmatic event developed in the Eastern Sierras Pampeanas (the Achalian magmatism; Dahlquist et al., 2014; Sims et al., 1998). Skirrow et al. (2000) assigned to this period the emplacement of auriferous and polymetallic veins in several districts of the Sierras Pampeanas, including Río Candelaria, San Ignacio and El Guaico, situated in the Sierra Grande de Córdoba (Fig. 1b). Although this regional metallogenic epoch was later proposed to be extended to Carboniferous times (Mutti et al., 2005), no Carboniferous ages have been reported for this mineralization style in the Sierras de Córdoba.

The geological and tectonic setting of the Late Paleozoic is subject of ongoing discussion. Recent lines of investigation involving the Carboniferous evolution of the Eastern Sierras Pampeanas are mainly focused on: a) thermo- and geochronological constraints on the low-temperature cooling history of the basement, associated with active deformation and exhumation of deep metamorphic levels (Bense et al., 2017; Löbens et al., 2016; Löbens et al., 2011; Wemmer et al., 2011; Whitmeyer, 2008), b) petrogenetic studies of Early Carboniferous A-type granites (Alasino et al., 2012; Dahlquist et al., 2016; Dahlquist et al., 2013, 2010; Morales Cámera et al., 2016) and c) structural configuration and sedimentary history of the retroarc Paganzo basin (Astini et al., 2009; Astini and Del Papa, 2014; Enkelmann et al., 2014; Limarino and Spalletti, 2006; Limarino et al., 2006). In contrast, ore genesis has been poorly studied and, therefore, its tectonic significance still remains unclear.

In this paper, we present geological data of polymetallic (Pb-Zn-Cu-Ag, Au) vein-type deposits from two little known districts, Las Guindas and Oro, situated in the Sierra de Comechingones, the southernmost range of the Sierras de Córdoba (Fig. 1b). These new results complement preceding works of Maffini (2015) and Maffini et al. (2017, 2012). Here, we combined field mapping, structural and kinematic analysis, evaluation of vein textures in relation to ore distribution and geochronological determinations by the K/Ar fine-fraction dating method on sericitic alteration. With this integrated information, we aim not only to temporally constrain the hydrothermal activity related to polymetallic mineralization, but also to evaluate the structural controls and deformation regimes involved during vein emplacement. Likewise, our interpretations are placed in the context of the Late Paleozoic tectonic evolution of the Sierras Pampeanas, making possible to evaluate the connection between deformation, magmatism, hydrothermal activity and sedimentation, in a still controversial geological setting.

2. The polymetallic (Pb-Zn-Cu-Ag ± Au) mineralization of the Sierra de Comechingones

The metamorphic basement of the Sierra de Comechingones (Fig. 1b) hosts several polymetallic vein-type deposits and minor occurrences that are exposed in a total N-S-trending area of approximately 1500 km^2. The region is dominated by Cambrian metasedimentary and metaigneous rocks, that have undergone high-grade metamorphism and partial melting during the thermal peak (700–800 °C and 7–8 kbar; Guereschi and Martino, 2008; Otamendi et al., 2004) of the first Paleozoic tectonic event, the Pampean orogeny, between ~550 and 520 Ma (Guereschi and Martino, 2014 and references therein; Rapela et al., 1998; Siegesmund et al., 2010). These Cambrian metamorphic sequences are reworked by the Ordovician- to Silurian Guacha Corral shear zone (Martino, 2003; Otamendi et al., 2004; Steenken et al., 2010), the widest mylonitic belt of the Sierras de Córdoba (Fig. 1b). Deformation along this shear structure, under ductile- to ductile-brittle conditions, was contemporaneous with the Famatinian orogeny (Collo et al., 2009; Ramos, 1988; Rapela et al., 2001; Thomas and Astini, 2003). The Guacha Corral shear zone is intruded in its central segment by the Devonian Cerro Áspero batholith (Pinotti et al., 2006; Pinotti et al., 2002), and to the north by the Achala batholith (Dahlquist et al., 2014; Lira and Kirschbaum, 1990; Rapela et al., 2008), the most voluminous granite intrusions of the Sierras de Córdoba (Fig. 1b) emplaced during the Achalian orogeny (Sims et al., 1998). These Pampean, Famatinian and Achalian orogenies, related to the collision and accretion of different

terranes along the proto-Pacific margin of Gondwana, strongly influenced the configuration of the Paleozoic basement of the entire Sierras Pampeanas, exposed now in the Andean foreland (Otamendi et al., 2004; Ramos, 1988; Rapela et al., 2007, 1998; Sims et al., 1998).

The quartz vein systems hosting Pb-Zn-Cu-Ag ± Au mineralization of the Sierra de Comechingones are invariably emplaced in metamorphic rocks, within or immediately adjacent to the Guacha Corral shear zone, showing a distribution in the vicinity of the Devonian plutons (Fig. 1b). The most representative mineralized areas comprise, from north to south, three main districts: Oro, Las Guindas and Piedra Blanca (Fig. 1b). The individual deposits in these districts are of relatively small size and show similar geological features. Although these areas were targets of prospecting and exploration between the 1940's and 1980's, only a few deposits were exploited by small-scale mining activities. Even though, no historical data is registered about reserves and production.

2.1. Structural characterization of ore vein systems in the Las Guindas and Oro districts

In the two selected study areas, Las Guindas and Oro districts, local mapping and structural analysis of individual deposits were combined to evaluate the role of different discontinuities and deformation regimes during ore vein deposition. The mineralized vein systems in the Sierra de Comechingones lack direct kinematic indicators (e.g. striations). In both districts, investigations were restricted to surface outcrops and, more rarely, to old exploration cores.

2.1.1. Orientation and along-strike continuity

The Las Guindas district is made up of two major mineralized NNW-trending shear structures, namely Guindas-I and Guindas-II, whereas a third structure of similar orientation and considerably minor extent, Guindas-III, was also recognized in the area (Fig. 2a). These major structures are mostly composed by an interconnected network of discontinuous ore quartz veins and veinlets, enclosing wall-rock fragments and forming narrow mineralized zones with an average width of 5 m and a maximum of 20 m. The vein segments, of variable length up to 100 m and frequent bifurcations from north to south, link to form a larger through-going structure which extends up to ~4 km in the case of the Guindas-I, and 2.5 km in the case of the Guindas-II (Fig. 2a). The most important past-producing mine of the district for Pb-Ag-(Au), the *Natacha* mine, is located at the NW tip of the Guindas-II (Fig. 2a).

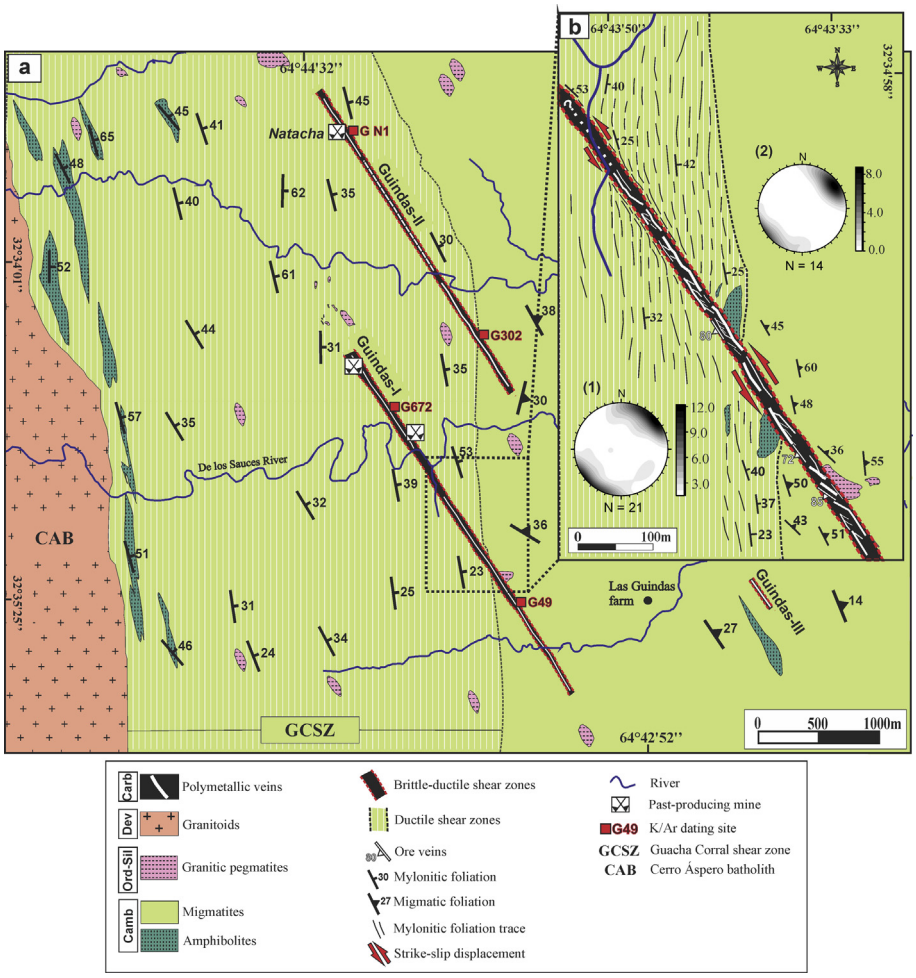

Fig. 2. a) Geological map of Las Guindas district showing the disposition and proved extent of the major mineralized structures. Sample locations for K/Ar dating are marked in the figure. b) Detailed scheme of a segment of the Guindas-I deposit showing the main structural and kinematic features. Notice how this structure intersects and sinistrally displaces the boundary between the Guacha Corral shear zone and the migmatic domain. Also observe the discontinuity and repetitive bifurcations of several vein segments, as well as their cross-cutting relationships with the surrounding planar structures of the host rocks. Two contoured pole diagrams (equal area stereonet projection, lower-hemisphere) showing the orientation of quartz ore veins and veinlets, hosted both in the Guacha Corral shear zone (plot n° 1) and in less to non-deformed migmatites (plot n° 2), are presented for this area. Notice the similarity of the diagrams despite the significant differences in the deformation fabrics of the host rocks. Also notice the meter-scale drag folds in the host rock foliation indicating a sinistral sense of strike-slip movement, and even how this kinematic pattern is evidenced by the river deflection (NW top).

The Guindas-I and Guindas-II structures cross-cut mylonitic rocks of the Guacha Corral shear zone and undeformed migmatites, as well as several scattered bodies of granitic pegmatites (Fig. 2). Migmatites exhibit a dominant NNW-striking foliation with moderate to gentle dip to the NE (mean foliation 338°/47°NE; Fig. 3), which is overprinted within the Guacha Corral shear zone by a strong penetrative mylonitic E-ENE-dipping foliation, with slightly variable strikes from NNW to NNE (mean foliation 354°/36°ENE; Fig. 3). Both migmatic and mylonitic foliations markedly contrast with vein orientations (Fig. 2 and Fig. 3). Although the intensity of deformation and strain fabrics are notably distinct in these two basement domains, no significant differences in the orientation of the veins and mode of emplacement were observed. Only a few minor veinlets appear to exploit the stronger mechanical anisotropies of the mylonites, being sub-concordant with the regional foliation (Fig. 3).

The major mineralized veins show a dominant strike direction of ~320–330° and are sub-vertical or dip steeply to the SW (Fig. 3). A secondary set of steeply-dipping veins striking ~290–300° is also recognizable in both Guindas-I and Guindas-II structures. Likewise, a large number of minor veinlets are frequently developed between major veins, presenting more variations in strike and dip angles. The whole data set of veinlets shows two dominant strike directions of ~330° and ~300°, with dips ranging between 30° and 88° both to the SW and NE (Fig. 3). This last group comprising 300°-striking veinlets commonly display *en-échelon* geometries throughout major 330°-striking veins (Fig. 2b). Furthermore, other less frequent sets of narrow anastomosing veinlets were measured, with strikes of around 180°, 260–270° and 220–230° (Fig. 3).

In the northernmost portion of the Sierra de Comechingones, the Oro district comprises five quartz ore veins, Oro-II to Oro-VI, that are poorly exposed within Cambrian migmatitic rocks (Fig. 4). Mylonitic deformation is incipient in this area, though it is recognizable within interspersed and narrow N-trending ductile shear zones consisting of deformed migmatites or protomylonites. The mineralized structures are developed both within and outside these bands cross-cutting the metamorphic foliation planes, which show a variable strike from NNW to NNE, with moderate to gently dip towards the E (mean foliation 004°/43°E; Fig. 3). Quartz veins, in turn, have strike lengths up to 30 meters. The Oro-II veins strike ENE and show a moderate to steep dip to the NNW, whereas the Oro-III comprises subvertical veins and veinlets striking WNW (Fig. 3). On the other hand, the Oro-IV and Oro-V structures present a dominant E-ENE strike and are mostly subvertical or dip steeply towards the S. Internal NW-striking veinlets are frequently developed within these major E-ENE veins or fracture zones following *en-échelon* patterns.

2.1.2. Kinematic analysis

Strain fabric and 3-D kinematic analyses were performed to determine the principal kinematic axes of the deformation regime

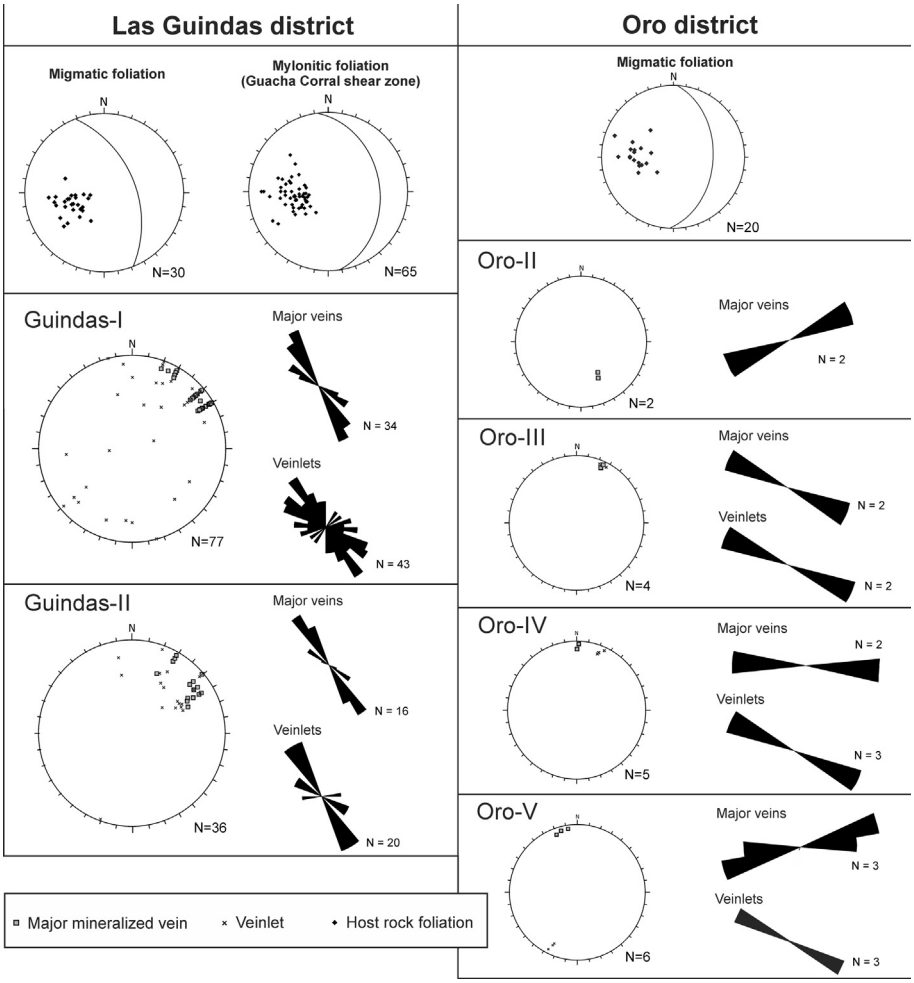

Fig. 3. Stereonet plots (equal area projection, lower-hemisphere) and rose diagrams showing the orientation of quartz veins and veinlets in the Las Guindas and Oro districts. Notice the high frequency of NNW- to NW-striking veins. The projection of the host rock foliation in the two basement domains is shown in stereonets at the top, including the mean foliation plane depicted with a solid great circle.

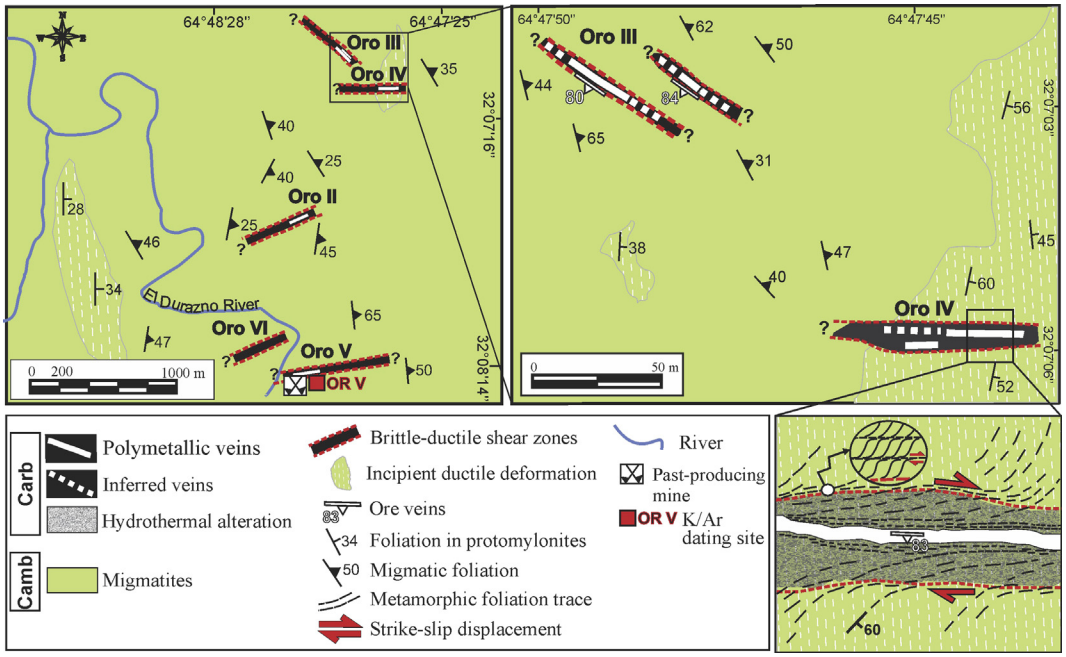

Fig. 4. Simplified geologic map of the Oro district with the location of mineralized structures and detailed views of the Oro-III and Oro-IV veins. Sample location for K/Ar dating is indicated. Notice in the inset (lower right corner) the meter-scale drag-folds in host rock foliation and *s-c* shear fabrics indicating dextral sense of strike-slip movement.

as well as direction and sense of slip along major mineralized structures, following the methodology outlined by Japas et al. (2013). Kinematic indicators were measured in brittle-ductile shear zones (in the sense of Ramsay and Huber, 1987), displaying tensional fractures. Passive markers (e.g. drag folds of the wall-rock foliation) and shape-preferred orientation of quartz crystals were locally considered. Data analysis and statistical procedures were carried out using the FaultKin 6.0 software (Allmendinger, 2001; Allmendinger et al., 2012), on the basis of concepts and methods provided by Angelier (1984) and Marrett and Allmendinger (1990).

In the Las Guindas district, mineralized sinistral brittle-ductile shear zones of meter-scale widths seem to be the dominant structures (Fig. 2). Steeply dipping 330°-striking vein segments with internal *en-échelon* minor veins and veinlets striking ~300° with variable dips, are the most common geometries used as kinematic indicators (Fig. 5a, b). Considering criteria from Dewey et al. (1998), Japas et al. (2013) and Sanderson and Marchini (1984), the <45° angles between main vein systems and tensional minor structures reveal a component of extension together with strike-slip deformation (Fig. 5b). Furthermore, a consistent sinistral sense of movement along the mineralized NNW-trending shear zones is also evidenced by drag folds in the wall-rock foliation, which tends to become parallel to vein orientation in strike and dip (Fig. 2b). The major Guindas-I structure displaced the N-trending contact between the Guacha Corral shear zone and the migmatic complex, resulting in a sinistral strike-slip motion of approximately 120 m along the shear plane (Fig. 2b).

The results of kinematic analysis are represented in Fig. 6 and reveal a N- to NNE extension direction (X) and W- to WNW shortening direction (Z) for both Guindas-I and Guindas-II mineralized structures (Fig. 6a). Steeply dipping Y axes and nearly subhorizontal X and Z axes (Fig. 6a) evidence a predominance of the strike-slip component along the major NNW-trending shear zones. Furthermore, the sub-parallel orientation of one of the nodal planes (striking at ~320°) with respect to the main direction of mineralized veins (see Fig. 3) supports this interpretation. On the other hand, results from fault-slip data (Fig. 6b) confirm subordinated components of normal dip-slip for most mineralized NNW-striking brittle-ductile shear zones, though minor reverse slip motions are recorded in three cases of NW-striking structures in both Guindas-I and Guindas-II.

Though scarce, kinematic indicators in the Oro district mostly comprise mineralized dextral E- to ENE-striking shear zones (Oro-IV and Oro V) with internal *en-échelon* tensional veinlets striking ~300° (Fig. 5c). Dextral displacements along these structures are also indicated by drag-folds of the wall-rock foliation and *s-c* shear fabrics (Fig. 4). The obtained kinematic axes are similar to those obtained for the Las Guindas district. A NE direction of extension (Fig. 6a) is supported by the low angles (<45°) between the E-striking shear zones and their internal NW-striking minor structures in addition to the presence of elongated quartz crystals within these tensional veinlets (see section below), showing wall-perpendicular growth (Fig. 5c). Fault-slip data in this district (Fig. 6b) also demonstrate a subordinated normal dip-slip component together with strike-slip motions along the major mineralized ENE-trending shear zones.

2.2. Vein textures and mineralization

Analysis of infill textures and composition of the veins was used to evaluate the relation between fracture sets and distribution of the ores. At least two quartz generations are recognizable. Barren milky quartz of massive to crustiform texture (quartz-1) infills both major and minor fractures of different oriented sets. Within major veins, it mostly occurs as subhedral and euhedral coarse grains showing a variable degree of intracrystalline deformation. Low-temperature deformation microstructures are observed in single crystals with predominance of fine- to wide extinction bands patterns (Derez et al., 2015), where *en-échelon* geometries are often developed at the tips of these bands (Fig. 7a). In less deformed tensional veinlets, quartz-1 crystals frequently are elongated in the direction of opening and perpendicular to the veins wall (Fig. 5c).

In contrast, the sulfide-rich and Ag-Au-rich vein infill is characterized by the injection of a distinct mineralized white to grayish

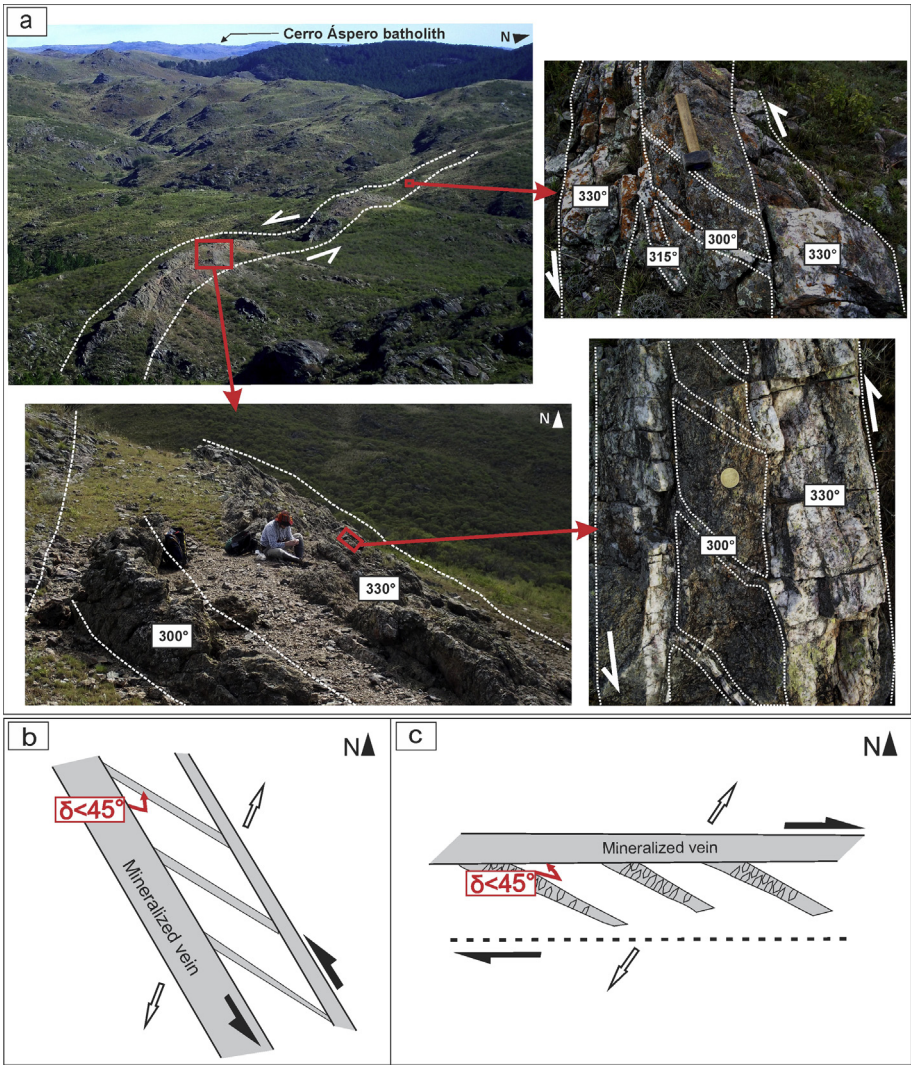

Fig. 5. Kinematic indicators. a) Field examples from the Guindas-I deposit showing at variable scale the development of internal *en-échelon* ~300°-striking minor veins and veinlets within the major 330°-trending structures. The strike values of each vein/veinlet set are correspondingly indicated in the pictures. The arrows on both sides of the thickest veins indicate the inferred sense of strike-slip movement. b) and c) Schematic geometrical relationships and kinematics inferred for the mineralized sinistral-normal NNW-trending shear zones of the Las Guindas district, and dextral-normal E-trending shear zones of the Oro district, respectively. Notice the low angles (<45°) between tensional veinlets and major veins of the zone boundary, as well as the strike-slip and extension directions. The sense of movement along the mineralized shear zones is given by the orientation and asymmetry of minor structures following *en-échelon* patterns. Also notice in the scheme (c) the quartz crystals within *en-échelon* tensional veinlets, showing a preferred shape elongation parallel to the direction of dilatation and perpendicular to the veins wall.

fine-grained quartz (quartz-2) into shear microfractures and void spaces, accompanied by subordinated amounts of sericite (Fig. 7b, c and d). Evidence of cracking, brecciation as well as resorption of quartz-1 crystals, caused by this episode of metallic ore mineralization, are usually recognizable at the microscopic scale. Preliminar fluid inclusion studies revealed similar homogenization temperatures in the primary and pseudo-secondary inclusions of both quartz-1 and quartz-2 varieties, into a range of 180–320 °C. Indeed, over 90% of the vein segments are made up of both types of quartz and frequently host weak to moderate disseminated metallic mineralization. However, there are some ore-rich sites where mineralization appears to be strongly concentrated, preferentially within zones of very intense brittle fracturing of the host rocks. Some of them constitute past-producing mines in the studied districts (Fig. 2a and Fig. 4). The spatial distribution of these sites does not seem to follow a specific control on surface. In some cases, they show a close affinity with tensional veins striking 300° but, in general, their occurrence is rather irregular along the extent of the major structures striking 330°.

Two main primary ore mineral assemblages were defined by Maffini (2015), based on microscopic studies of polished sections, EDS (Energy Dispersive Spectrometry) and EMPA (Electron Microprobe Analysis) data: (1) a purely sulfide assemblage with pyrite, galena, sphalerite, chalcopyrite and scarce tetrahedrite; and (2) a Te-rich assemblage with (still) dominant sulfide mineralogy but in association with Te-Ag-Au-bearing minerals. In the Las Guindas district, Hessite (Ag_2Te), Cervelleite (Ag_4TeS) and Petzite (Ag_3AuTe_2) are the main telluride species which occur as intergrown grains associated with pyrite, whereas in the Oro district the tellurides were mostly observed as complex polyphase grains associated with galena. Although the paragenetic relationships between both mineral assemblages are difficult to examine with only surface mineralogical data, the deposition of tellurides traditionally takes place after the initial deposition of sulfides in most meso- and epithermal systems (Afifi et al., 1988).

Non-systematic precious metal analyses performed on mineralized samples from the Las Guindas district (by the fire-assay/atomic-absorption method; Maffini, 2015) revealed widely

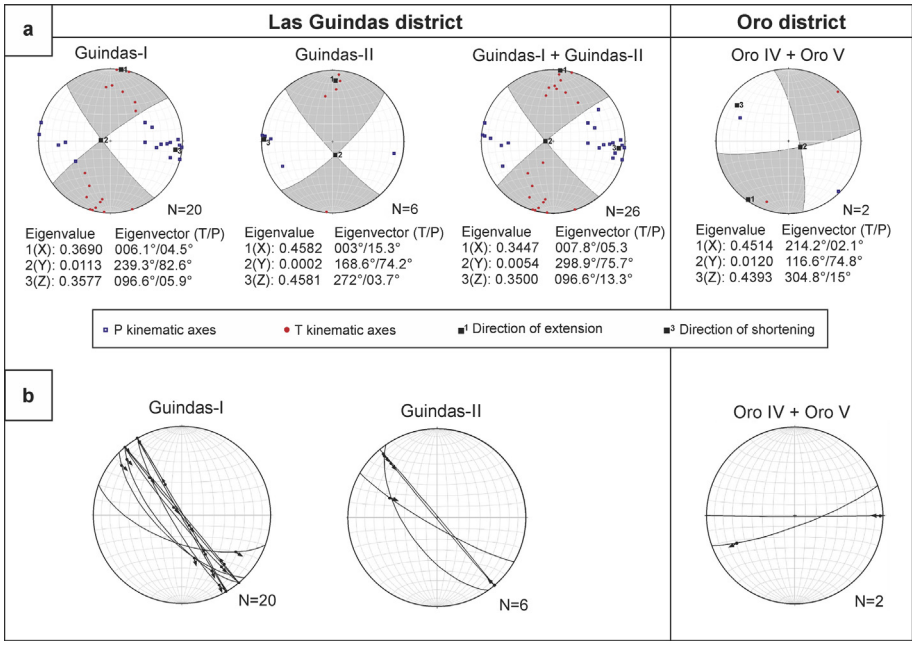

Fig. 6. Graphical representation of the kinematic analysis in the Las Guindas and Oro districts obtained using the FaultKin 6.0 software (Allmendinger, 2001; Allmendinger et al., 2012). a) 3-D kinematic plots showing the estimated kinematic axes. "T" and "P" represent the infinitesimal extension and shortening axes, respectively, for each individual measured structure. Two nodal planes delimit the extension (gray area) and shortening (white area) fields, whereas the main kinematic axes X, Y and Z (linked Bingham axes) represent the average orientation (Trend/Plunge) of the principal incremental strain (Marrett and Allmendinger, 1990). Notice the coherent results obtained for the two studied districts (see more explanation in text). b) Fault-slip diagrams (equal-area, lower-hemisphere projection) displaying the orientation of individual measured mineralized structures (great circles). Solid dots and arrows represent the relative slip direction of the hanging-wall side of the corresponding structure.

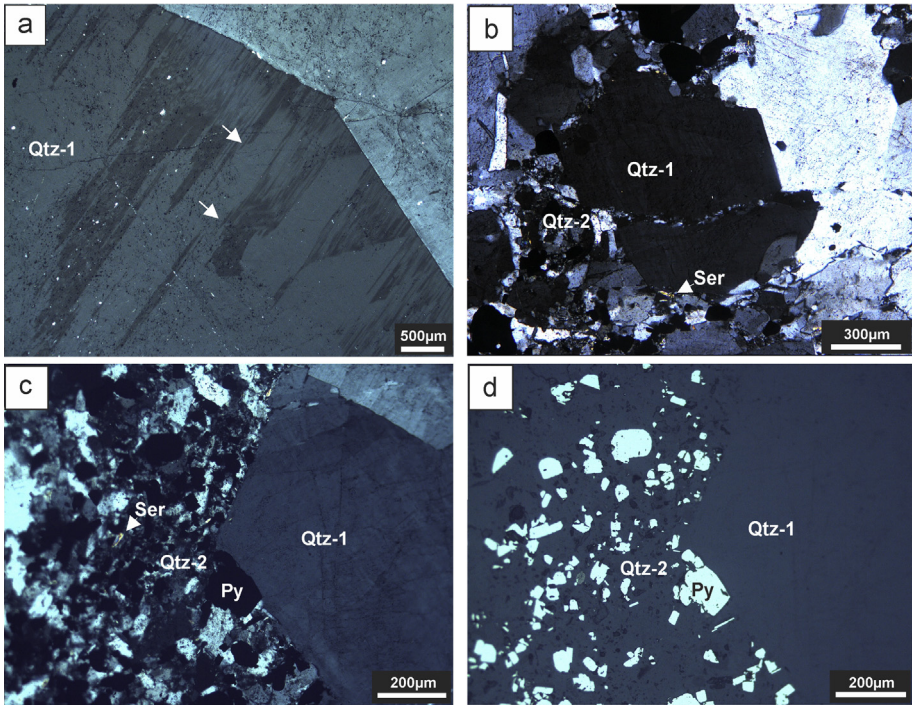

Fig. 7. Main petrographic textures and microstructures related to quartz-ore deposition. a) Low-temperature deformation microstructures consisting of fine- to wide extinction bands in the barren quartz type (Qtz-1). Notice the *en-échelon* arrangement developed at the tip of these bands (some indicated by white arrows). b) Brittle cracking of a Qtz-1 crystal caused by the injection of the mineralized fine-grained Qtz-2 into a shear microfracture. c), d) Transmitted and reflected light views showing the sulfide-rich Qtz-2 filling void spaces between Qtz-1 coarse grains. Notice how the upper part of the large euhedral crystal undergoes brittle deformation and partially breaks. In this section, pyrite is the most abundant sulfide, containing very small inclusions of Ag-Au tellurides, which are not visible at the scale of the picture.

variable Ag and Au contents at different vein segments. In areas with weak disseminated metallic mineralization, Ag content can range from <2 to 45 g/t and Au from <0.03 to 0.43 g/t, whereas in the ore-rich sites Ag and Au contents can reach up to 216 g/t and 10.54 g/t, respectively. The precious metals always show a positive correlation with base metals, such as Pb, Zn and Cu (Maffini, 2015). These portions where metallic mineralization is largely concentrated usually manifest a significant degree of supergene oxidation, with abundant *boxwork* textures and secondary mineral phases. Current available metal chemistry data from the Oro district are restricted to previous prospecting studies of Miró and Candiani (1985), who reported an average content of 80 g/t Ag and 4 g/t Au, without sampling or method specifications.

2.3. Wall-rock alteration

Hydrothermal alteration is structurally controlled and restricted to continuous zones of 1–5 m width close to the veins. It mainly consists of penetrative and widespread sericitization of the mylonitic and migmatic host rocks and local carbonatization (siderite-calcite) of interspersed amphibolites. A distal and subordinated chlorite ± sericite alteration (by chloritization of biotite and/or amphibole) can be recognized in some altered zones.

The hydrothermal sericite occurs as fine-grained aggregates, which partially or totally overprint the metamorphic paragenesis (Fig. 8). This alteration is, in turn, usually more extensive and intense within mylonitic areas than within non-deformed areas, probably in response to a higher permeability. The paragenetic relationship between sulfide-rich quartz (quartz-2) and sericite is clear within the veins, even though it is no possible to unequivocally ascertain that sericitization of the wall-rock was only restricted to the episode of metallic ore deposition.

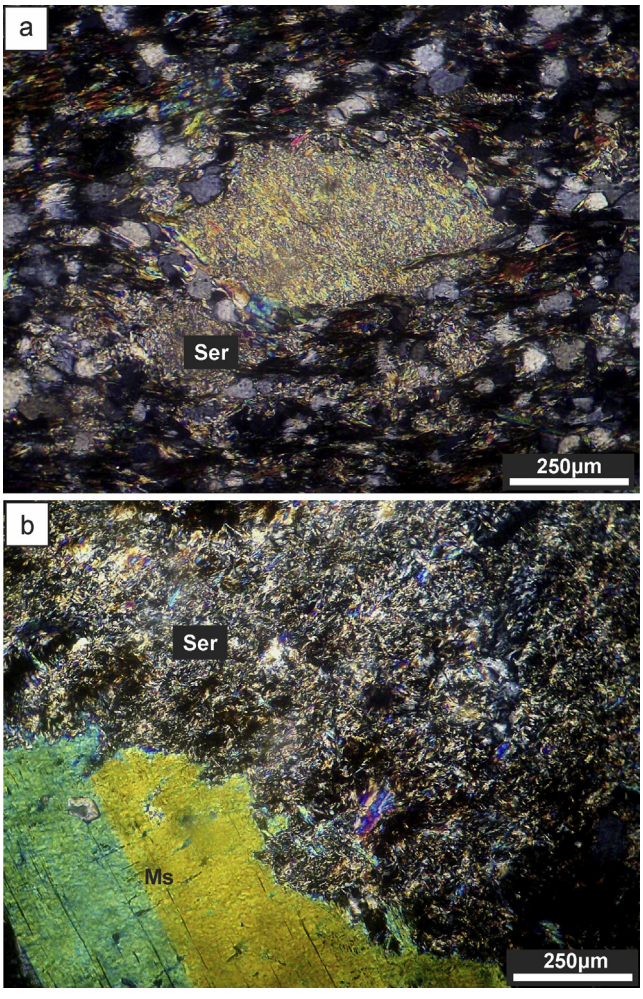

Fig. 8. Hydrothermal sericite alteration (photomicrographs in cross-polarized light). a) Total replacement of feldspar porphyroclasts by fine-grained hydrothermal sericite (Ser) in a mylonite from the Guacha Corral shear zone. Abundant biotite grains of the matrix were also totally sericitized. b) Partial replacement of relic metamorphic coarse muscovite (Ms) by hydrothermal sericite in a protomylonite close to the eastern boundary of the Guacha Corral shear zone. The two mica fractions from this sample (G302) were dated by the K/Ar method, yielding a Silurian age for the coarse-grained muscovite and a Carboniferous age for the fine-grained sericite (see data in Table 1).

2.4. K/Ar dating of hydrothermal white mica

In order to constrain the timing of the hydrothermal activity in the Las Guindas and Oro districts, five samples of the sericite-bearing alteration zones were dated by the K/Ar fine-fraction method (Clauer, 2013; Clauer and Chaudhuri, 1995). In the Las Guindas district, four samples from the northern and southern segments of both Guindas-I and Guindas-II major veins were taken (see sample location in Fig. 2a), whereas in the Oro district one sample was taken from the Oro-V vein (sample location in Fig. 4). All the samples were collected less than 30 cm from vein contacts, where hydrothermal alteration is intense.

2.4.1. Sample preparation and data acquisition

At least 1 kg of rock material per sample was crushed, gently ground in a shatter mill (for 12–15 s) and split by sieving into grain sizes >63 μm and <63 μm. An additional fraction >250 μm was isolated from the sample G302 (Guindas-II structure; Fig. 2a) in order to enrich and subsequently separate the metamorphic coarse-grained muscovite. The fractions <63 μm were used to extract the fraction <2 μm by differential settling in Atterberg cylinders. The obtained concentrates were subjected to isotope measurements and X-ray diffraction (XRD) analyses for determination of the illite crystallinity, mineralogical composition and illite polytypes. All laboratory and analytical procedures were carried out at the Geoscience Centre of the George-August University of Göttingen.

The XRD analyses were performed using a Philips PW 1800 diffractometer equipped with a copper-target tube operating at 45 kV and 30 mA. The illite crystallinity was determined on textured preparations under air-dried and ethylene glycol saturated conditions by measuring the full width at half maximum height of the 001 peak at 10 Å. The samples were step-scanned from 7 to 10° 2θ at 0.01° 2θ steps with a counting time of 4sec/step and the illite crystallinity is expressed as illite Kübler index (KI; Kübler, 1967) using the software IDEFIX by Friedrich (1991). XRD determinations on randomly oriented powders were also carried out to monitor the mineralogical composition and illite polytypes. The step scan conditions were extended from 4 to 65° 2θ at 0.02° 2θ steps with a time of 12 sec/step. The XRD profiles were analyzed by using the PANalytical X'Pert HighScore Plus software version 2.1. Polytype identification was made using the relative intensities at 3.88, 3.72, 3.49, 3.2, 2.98, 2.86 and 2.78 Å for the polytype $2M_1$ and 3.07 and 3.66 Å for the 1M (Drits et al., 1993; Moore and Reynolds, 1997). Relative proportions between polytypes were qualitatively assessed by comparing the obtained XRD patterns with end-members and intermediate standards from the Owl Creek pegmatite (Wyoming, USA) and the Silver Hill Formation (Montana, USA), evaluated and characterized by Haines and van der Pluijm (2008).

The argon isotopic composition was measured in a pyrex glass extraction and purification line coupled to a Thermo Scientific ARGUS VI™ noble gas mass spectrometer, operating in static mode. The amount of radiogenic ^{40}Ar was determined by isotope dilution

Table 1
Summary of K/Ar results, Kübler indexes, illite polytypes and mineral composition of the analyzed hydrothermal fractions < 2 μm. K/Ar data for the mica fraction > 250 μm is also included. Minerals in each sample are indicated in order to their relative abundance: (++) Principal component, (+) Abundantly present or only in traces. Mineral abbreviations: Gth = goethite, Ill = illite, Kao = kaolinite, Qtz = quartz, Rt = rutile.

Sample (lat/long coordinates)	Grain Fraction (μm)	K/Ar data					Illite crystallinity (Δ°2θ)		Illite polytype	Mineral components
		K_2O (wt.%)	$^{40}Ar^*$ (nl/g) STP	$^{40}Ar^*$ (%)	Age (Ma)	±2σ error (Ma)	Air dried	Glycol.		
G672 (32°34′40″ S 64°44′06″ W)	<2	9.40	109.43	98.83	**329.2**	5.8	0.216	0.216	$2M_1$ 1 M	Ill (++) – Qtz (+) – Gth (+) – Rt (+)
G49 (32°35′23″ S 64°43′29″ W)	<2	7.63	84.86	98.78	**315.7**	3.7	0.216	0.212	$2M_1$ 1 M	Ill (++) – Qtz (+) – Gth(+) – Rt(+) – Kao (+)
GN1 (32°33′34″ S 64°44′17″ W)	<2	8.74	99.38	98.85	**322.0**	3.9	0.232	0.225	$2M_1$ 1 M	Ill (++) – Qtz (+) – Gth(+) – Rt(+)
G302 (32°34′28″ S 64°43′39″ W)	<2	7.72	89.35	98.56	**327.3**	3.9	0.231	0.223	$2M_1$ 1 M	Ill (++) – Qtz (+) – Gth (+) – Rt (+)
	>250	11.29	173.70	97.90	**423.3**	4.2	–	–	–	
OR V (32°08′14″ S 64°48′03″ W)	<2	7.19	81.00	98.32	**319.3**	4.2	0.201	0.202	$2M_1$ 1 M	Ill (++) – Qtz (+) – Rt (+) – Kao (+)

method using a highly enriched ^{38}Ar spike from Schumacher, Bern (Schumacher, 1975). The spike was calibrated against the biotite standard HD-B1 (Fuhrmann et al., 1987) and the age calculations were based on the constants recommended by the IUGS quoted in Steiger and Jäger (1977).

Potassium was determined in duplicate by flame photometry using a BWB-XP flame photometer™. The samples were dissolved in a mixture of HF and HNO_3 according to the technique of Heinrichs and Herrmann (1990). The analytical error for the K/Ar age calculations is given on a 95% confidence level (2σ). Details of argon and potassium analyses for the laboratory in Göttingen are given in Wemmer (1991).

2.4.2. Results and interpretation

The obtained geochronological data as well as the XRD results are summarized in Table 1 and Fig. 9. The separated fractions <2 μm are all enriched in illite with only minor amounts of other minerals. Impurities of quartz and rutile are typically present in all the samples, whereas goethite and kaolinite were detected in some of them. The Kübler index (KI) does not show significant variations and ranges from 0.201 to 0.232 Δ°2θ, indicating a relatively high crystallinity of the illite. These values correspond to conditions near the anchizone/epizone boundary around 300 °C in the zonation scheme of Kübler (1967) and Verdel et al. (2011). The presence of expandable-layer clays (e.g. smectite) was excluded, based on the small differences between the air-dried and ethylene glycol saturated measurements (Table 1). Nevertheless, the XRD analyses of random powders confirm the physical mixture of $2M_1$ + 1M illite polytypes in all the samples (Table 1; Fig. 9a). By comparing the intensity and width of characteristic reflection peaks, the proportion ratio between both polytypes does not seem to vary markedly in the analyzed samples, this being fully consistent with the almost constant KI values. The mixture of $2M_1$ and 1M illites may possibly reflect progressive stages of crystallization during the evolution and cooling history of the hydrothermal system, resulting in a transition from $2M_1$ to 1M polytypes. Another likely explanation, however, could be attributed to differences in composition. As it was previously demonstrated by other authors (Peacor et al., 2002; Velde, 1965a,b), both polytypes can grow at the same time fostered by compositional variations in some hydrothermal systems. In this sense, crystallization of $2M_1$ and 1M illites may not be related to a specific event, but rather to distinct physico-chemical conditions during fluid-rock interaction. Despite of being speculative, it could be possible if considering the usual compositional variations of the hydrothermal white micas, from potassic to phengitic, already reported by Maffini et al. (2017). Nevertheless, there is no conclusive indication if these proportional mixtures of $2M_1$ and 1M polytypes are closely related to the temperature of illite formation or rather to compositional factors, thus, both scenarios should be considered.

The K/Ar analyses of the fractions <2 μm yielded Carboniferous ages (Fig. 9b). In the Las Guindas district, two main groups of K/Ar ages can be recognized. The oldest correspond to Late Mississippian ages (ca. 329–327 Ma) and are recorded in samples from the Guindas-I and Guindas-II veins, respectively. The youngest group is represented by Early Pennsylvanian ages (ca. 322–315 Ma) also registered in both mineralized structures. Furthermore, the age around 319 Ma recorded in the Oro district is certainly an intermediate age between both members of the second group. Such distribution shows that the majority of the ages overlap within error between ~322 and 325 Ma. On the other hand, the coarse-grained fraction (>250 μm) dated from sample G302 yielded a onsiderably older age of 423.3 ± 4.2 Ma (Late Silurian; Table 1), consistent with several petrographic and textural observations where fine-grained hydrothermal white mica overprints the relic metamorphic muscovite (Fig. 8b).

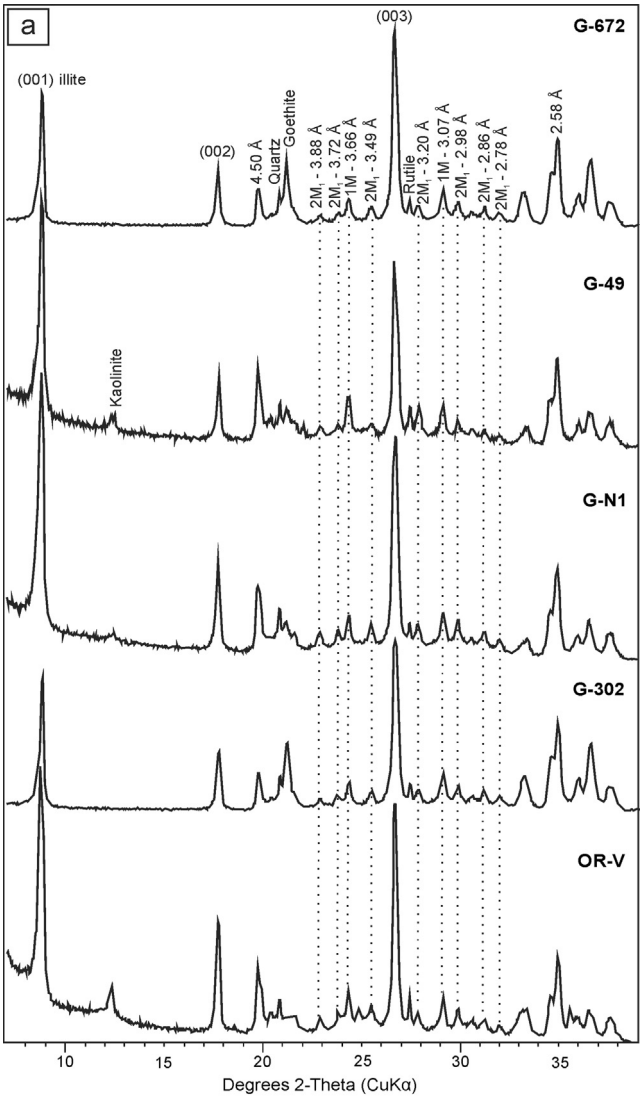

The interpretation of the K/Ar ages requires the understanding of the temperature at which the white micas are closed to argon diffusion (Kelley, 2002; Villa, 1998). Minerals grown below their closing temperature yield crystallization or formation ages, while the ages obtained on minerals grown under higher temperatures have to be interpreted as cooling ages representing the minimum age for the formation of the paragenesis. For decades, this temperature has been estimated to be 350 ± 50 °C according to Purdy and Jäger (1976). More recently, Harrison et al. (2009) calculated a closure temperature of 425 °C for muscovites with 100 μm radius, which is now widely accepted. As the closing temperature depends on the effective grain size, it should be lower for <2 μm fine fractions, because of shorter diffusion path ways. Hunziker et al. (1986) published a closure temperature for muscovite fractions <2 μm of 260 ± 30 °C, while Wemmer and Ahrendt (1997) stated that 270 °C are definitely not enough for a total reset of the isotope system and suggested a closure temperature between 260° and 350 °C for mineral fine fractions.

Considering the evidence from mineral assemblages, illite crystallinity and polytypes, deformation microstructures in quartz and preliminar fluid inclusions microthermometry, suggesting that temperatures in the hydrothermal system did not exceed ~320 °C, we interpret the K/Ar ages as the approximate crystallization age of the newly formed hydrothermal white mica (<2 μm). However, we do not totally exclude the possibility of partial loss of argon to some extent in the finest fractions during cooling of the hydrothermal system and the feasible transition from $2M_1$ to 1M illite varieties, which could have given rise to slightly younger ages. On the other hand, K/Ar ages are unlikely to represent mixtures between the hydrothermal alteration and older crushed micas from the metamorphic host rocks, since these components were ruled out within the separated fine-grain sizes, as it was confirmed by XRD data. If some muscovite from the host rock were present, it would be identified by its crystallinity (~0.060 Δ°2θ; Wemmer, 1991) Furthermore, the presence of kaolinite in some of the sample material is also unlikely to disturb the isotopic system, as this mineral does not contain K or Ar, and its origin is restricted to the chemical weathering of feldspars.

3. Discussion

3.1. Structural controls on ore deposits

The structural elements preserved in the studied ore deposits represent a distinctive structural and kinematic style within the Early- to Middle Paleozoic metamorphosed basement of the Sierra de Comechingones. Steeply dipping brittle-ductile shear zones with associated *en-échelon* tensional fractures seem to be the dominant structures in the Las Guindas and Oro districts, through

Fig. 9. Graphic representation of X-ray diffraction and geochronological data. a) X-ray diffraction patterns of the separated illite-rich fractions <2 μm. The interpretation of characteristic reflection peaks of minerals and illite polytypes ($2M_1$ and 1M) is shown in the figure. b) Summary of Carboniferous geochronological data from the Sierras de Córdoba including the obtained K/Ar fine-fraction ages. The time range assigned to the Early Gondwana Magmatism of the Eastern Sierras Pampeanas (Alasino et al., 2012; Dahlquist et al., 2010, 2013, 2016) is shown as a vertical rectangle with dashed lines. The limits between early (E), middle (M) and late (L) Mississippian and Pennsylvanian epochs were taken from the International Chronostratigraphic Chart (2016), available on the *International Commission on Stratigraphy* webpage. Data Sources: (1) This work; (2) Steenken et al. (2010); (3) Dahlquist et al. (2016); (4) Gómez (2003).

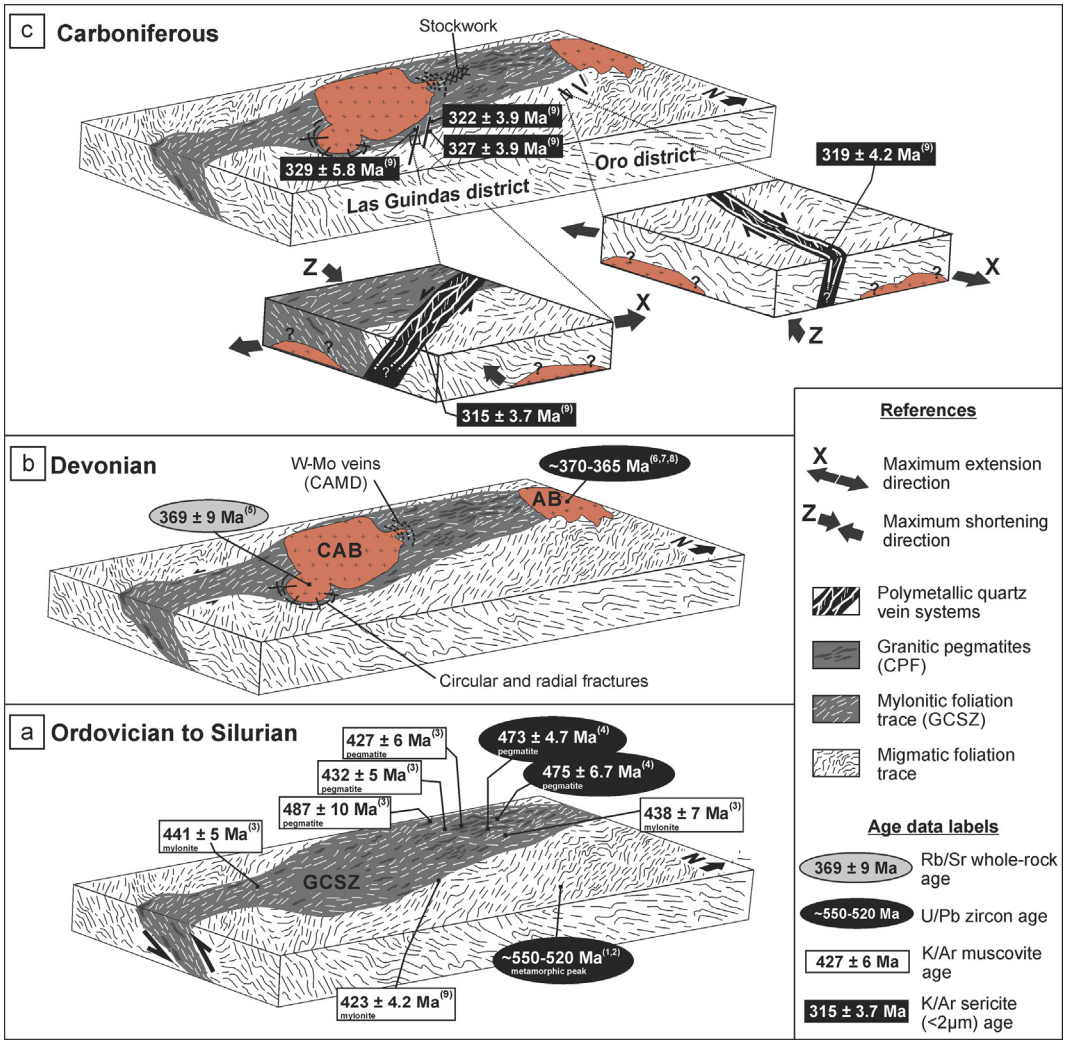

Fig. 10. Geological sketch showing the Middle- to Late Paleozoic evolution of the Sierra de Comechingones, with special emphasis on the principal deformation structures in the basement, and the associated magmatism and metallogenesis. Age data sources: (1) Guereschi and Martino (2014 and references therein); (2) Siegesmund et al. (2010); (3) Steenken et al. (2010); (4) Demartis et al. (submitted for publication); (5) Pinotti et al. (2006); (6) Dahlquist et al. (2014); (7) Dorais et al. (1997); (8) Rapela et al. (2008); (9) This work. Abbreviations in the figure: AB = Achala Batholith; CAB = Cerro Áspero Batholith, CAMD = Cerro Áspero Mining District; GCSZ = Guacha Corral Shear Zone, CPF = Comechingones Pegmatitic Field.

which the hydrothermal fluids were preferentially channelled. Structural and kinematic data demonstrate that strike-slip deformation played a major role during vein emplacement, with a sinistral sense of shear along the principal mineralized NNW-trending structures (Las Guindas district) and dextral shear along E- to ENE structures (Oro district). However, minor components of normal-slip movements were corroborated by fault-slip data for the majority of the brittle-ductile shear zones (Fig. 6b), defining a transtension regime (*Transtension* in the sense of Dewey et al., 1998; Fossen and Tikoff, 1998; Sanderson and Marchini, 1984). The <45° angles between major vein systems and multiple sets of tensional minor structures (Fig. 5) further support a component of extension together with strike-slip deformation (Japas et al., 2013; Sanderson and Marchini, 1984). Nevertheless, reverse-slip was found in some NW-trending segments of the shear zones in the Las Guindas district.

Hence, we interpret that NNW-striking sinistral-normal brittle-ductile shear zones represent the main structural control on mineralization, whereas E- to ENE-striking dextral-normal shear zones comprise a less developed conjugated set. The compression (P) and extension (T) axes inferred from kinematic analyses (Fig. 6a) indicate a coherent kinematic pattern of the fracture systems, with a maximum extension direction (X) oriented NNE- to NE and maximum shortening (Z) oriented WNW- to NW. This structural arrangement for the Carboniferous is illustrated in Fig. 10 within the context of the Middle- to Late Paleozoic evolution of the Sierra de Comechingones (see section below).

A key structural aspect to also discuss is the role that the pre-existing anisotropies of the basement played during vein emplacement. Considering that large-scale shear zones behave as domains of crustal weakness, one of the initial hypothesis of this investigation was the control that the Guacha Corral shear zone might have had on strain accommodation. However, the strongly anisotropic mylonitic fabrics were not a critical control on the orientation and geometry of the brittle fracture planes. In fact, many of the ore vein systems are very well developed outside the mylonitic domain. The major steep-dipping mineralized structures cross-cut all earlier regional foliations and deflect them as passive markers. This is particularly clear in the Las Guindas district, where the 2.5- to 4 km-long mineralized structures sinistrally displace the NS-trending contact between the Guacha Corral shear belt and the undeformed migmatitic massif (Fig. 2b). Nevertheless, a possible control and transtensional reactivation of other pre-existing anisotropies of the basement is not here discarded. Similar sets

of major NNW- to NW-trending fractures were already described in the region as principal structural controls for the ascent and emplacement of granite magma in the Devonian batholiths, such as the Cerro Áspero in the Sierra de Comechingones (Pinotti et al., 2002) and Las Chacras in the Sierra de San Luis (Siegesmund et al., 2004). On the other hand, brittle structures resulting from reactivation of mylonitic and metamorphic foliations could be considered as well, though no regional data are available so far to evaluate this hypothesis.

Furthermore, field evidence indicates that the spatial distribution of the metallic ore is essentially independent of the vein geometries at the deposit scale. It is expected that larger amounts of hydrothermal filling and mineral deposition would have occurred at structurally favorable places within the transtensional zones, such as tensional veins and dilation sites. However, this control is not observed. Thus, the structural and kinematic data do not totally explain the variability in mineral assemblages and metal content within the veins. We interpret that this irregular and selective distribution of the ores may probably reflect independent and episodic fluid paths with variable concentration of metals, combined with differential movements within zones of intense fracturing during a transtensional deformation regime. Fluid flow should have been promoted and channeled by irregular opening of the host fractures. In turn, the higher permeability of the mylonitic zones is evidenced by a more intense sericite alteration of the wall-rocks. In this context, reverse osmosis can be an alternative to explain ore concentration, similarly as it has been postulated for porphyry metal zoning during the phyllic stage (Japas et al., 2015). Japas et al. (2015) suggest that reverse osmosis could be favored in a differential stress field that would enhance a differentiated permeation phenomenon through the phyllic halo at temperatures less than 335 °C.

3.2. Temporal and genetic connection between mylonitic deformation, magmatism and metallogenesis

The new obtained K/Ar ages point to a Carboniferous long-lasting episodic hydrothermal activity (~15 Ma) in the Sierra de Comechingones, which postdates a polyphasic deformation history of the basement (Fig. 10). The Ordovician to Silurian period, related to the Famatinian orogeny, was dominated by ductile to ductile-brittle deformation along the Guacha Corral shear zone (Fig. 10a; Demartis et al., 2011; Otamendi et al., 2004; Steenken et al., 2010). The K/Ar age of 423.3 ± 4.2 Ma (Late Silurian) obtained in our work in coarse-grained muscovite comprises a new cooling age recording mylonitic deformation in the eastern boundary of the shear zone. Interestingly, this age postdates the K/Ar age of ~439 Ma reported by Steenken et al. (2010) as the last phase of shear reactivation, related to the final collision of the Cuyania terrane at the western Gondwana margin. Likewise, thrusting along this crustal-scale mylonitic belt exerted a strong structural control on the emplacement of voluminous pegmatitic melts (Be-P-Nb-Ta-U) at middle crustal levels (*Comechingones Pegmatitic Field*, Demartis et al., 2011; Fig. 10a). The last authors determined a compressive stress field for this event with sub-horizontal Z and Y axes, oriented E-W and N-S, respectively.

The Guacha Corral shear zone was also a relevant control on the channeling and intrusion of Devonian granitoids through major fractures at shallow crustal levels (Coniglio, 2006; Pinotti et al., 2006; Pinotti et al., 2002). In turn, some authors (Mutti et al., 2007) invoked a sinistral sense of shear at the time of granite intrusion (Fig. 10b). The ascent of magma during the emplacement of the Cerro Áspero batholith generated a profuse set of circular and radial fractures conspicuously discordant to previous structures (Pinotti et al., 2002; Fig. 10b). The crystallization age of 369 ± 9 Ma determined for the Cerro Áspero batholith (Rb/Sr isochrone; Pinotti et al., 2006) overlaps the age range between ~370 and 365 Ma of the Achala batholith (U/Pb zircon ages; Dahlquist et al., 2014, 2013; Dorais et al., 1997; Rapela et al., 2008; Fig. 10b), thus placing this magmatism in the Late Devonian. Important magmatic-hydrothermal W-Mo-bearing deposits are hosted in many circular fractures at the northern tip of the Cerro Áspero batholith, comprising the past-producing Cerro Áspero Mining District (Coniglio, 2006; Coniglio et al., 2000; Mutti and González Chiozza, 2005; Fig. 10b). Accordingly, a Devonian metallogenic epoch spatially and temporally related to this major magmatism in the Sierras Pampeanas (the Achalian magmatism, Dahlquist et al., 2014; Sims et al., 1998), was constrained between ~390 and 360 Ma (Skirrow et al., 2000).

It is clear that the Carboniferous hydrothermal event of the Sierra de Comechingones (~329–315 Ma) significantly postdates the Devonian magmatism and its related metallogenesis. Most of the evidence thus allow ruling out a direct connection between the studied mineralization and the large Devonian batholiths, in spite of their relative spatial proximity. In fact, the Mississippian to Pennsylvanian ages obtained here largely fall within the age range of 357–322 Ma assigned by Dahlquist et al. (2016, 2013, 2010); and Alasino et al. (2012) to the A-type Early Carboniferous magmatism of the Eastern Sierras Pampeanas (also referred as *Early Gondwana magmatism*; Fig. 9b), and coincide with the Gondwana metallogenic epoch constrained for the Sierras de San Luis (Ulacco, 2001; Ulacco et al., 2005).

It is possible that the polymetallic mineralization is linked to the existence of non-exhumed granitic intrusions of presumed Carboniferous age at shallow depths (Fig. 10c). This hypothesis of buried young granites was already suggested by other authors based on field evidence (e.g. widespread quartz-pyrite stockworks at the north of the Cerro Áspero batholith, Boffadossi et al., 2016; Coniglio, 2006; Fig. 10c), as well as recent geophysical studies revealing noticeable gravimetric anomalies under the metamorphic basement (Radice et al., 2015). In addition, similar ideas were also proposed to explain hydrothermal activity in distinct areas of the Sierra Grande de Córdoba (e.g. in the El Guaico and Agua de Ramón districts, Biglia et al., 2016; de Brodtkorb et al., 2014; Lyons et al., 1997; see location in Fig. 1b). Hence, it is reasonable to suggest that many hydrothermal ore deposits and alterations in the Sierras de Córdoba could reveal the regional extent of a non-exposed younger (?) magmatism. These granites might have a possible geotectonic connection with the scattered outcrops of Carboniferous plutons of Córdoba (Fig. 1b), such as the Serrezuela (~322–303 Ma, K/Ar biotite, Fig. 9b; Gómez, 2003) or the Capilla del Monte (~336–337 Ma, U/Pb and Rb/Sr ages, Fig. 9b; Dahlquist et al., 2016), and even with other A-type granites of La Rioja and Catamarca provinces (Alasino et al., 2012; Macchioli Grande et al., 2015; Morales Cámera et al., 2016).

3.3. Tectonic setting at the time of metallogenesis: a distinctive Carboniferous phase?

Though the Early- to Middle Paleozoic tectonic evolution of the Sierras Pampeanas is well-constrained, the characteristics and significance of Carboniferous tectonics are still an open debate. Alasino et al. (2012) and Dahlquist et al. (2016, 2010) proposed that the emplacement of Early Carboniferous A-type granites of the Eastern Sierras Pampeanas took place in an extensional tectonic regime, in contrast to the compressional setting inferred for the Late Devonian batholiths of Córdoba and San Luis, related to the final stages of the Achalian orogeny (López de Luchi et al., 2004; Siegesmund et al., 2004; Sims et al., 1998; Stuart Smith et al., 1999). Consistently with the last authors, Skirrow et al. (2000) and Mutti et al. (2007) proposed compressional tectonics for Devonian mineralization of the Southern Sierras Pampeanas.

The transtensional deformation regime proposed in our study for the Carboniferous would support the idea of a non-compressive setting, even though no kinematic data are available for mineralizations of comparable age in the Sierras de Córdoba or in the Sierras de San Luis. A transtensional regime controlling Carboniferous magmatism and genetically linked mineralization was as well defined for the Fiambalá region at the northern Sierras Pampeanas (Hongn et al., 2010; Japas et al., 2004). The last authors proposed a kinematic evolution for that area and interpreted a sinistral transtensional regime during a period of postorogenic crustal relaxation. N-, NNW- and E-striking structures are also described as the most relevant mineralized systems. Thus, the subordinated transpressive mineralized brittle-ductile shear zones found in the Las Guindas district may probably reflect an emplacement very close to the transition between the Late Devonian compressional/transpressional orogenic setting (following Siegesmund et al., 2004; Sims et al., 1998; Skirrow et al., 2000) and the subsequent Carboniferous extensional/transtensional regime (following Dahlquist et al., 2010; Hongn et al., 2010; Japas et al., 2004). The orientation of kinematic axes in the two studied districts (Fig. 6a and Fig. 10c) supports this interpretation. The W- to WNW-trending Z axis in the Las Guindas district suggests a reactivation of the mineralized brittle-ductile shear zones from the beginning of the transtension, whereas the NW-trending Z axis in the Oro district may indicate a relatively later stage.

The Late Paleozoic post-metamorphic history of the Sierras de Córdoba also implied progressive cooling and exhumation of different basement domains during the Carboniferous, synchronously with active deformation under brittle conditions (Bense et al., 2017; Löbens et al., 2016, 2011; Steenken et al., 2010; Wemmer et al., 2011; Whitmeyer, 2008). This evolution of the basement was concomitant with the development of the retroarc Paganzo basin, whose sedimentation is recorded in the Sierras de Córdoba (Astini and del Papa, 2014 and references therein; see Fig.1b). This basin was interpreted as a suite of transtensional pull-apart depocentres linked along major strike-slip crustal faults (Astini et al., 2009; Fernandez-Seveso and Tankard, 1995), thus also pointing to a non-compressive tectonic setting for the Early Carboniferous.

Considering available data and new evidence presented here, we propose a distinctive Carboniferous deformational phase for the Eastern Sierras Pampeanas, dominated by transtension, in agreement with the recent hypothesis of Löbens et al. (2016). Further data are, however, required to constrain the time interval in which the compressive setting of the Achalian orogeny changed to a non-compressive one, in order to understand the early evolution of the proto-Andean margin of Gondwana.

4. Conclusions

Strain fabric and 3-D kinematic analysis performed here provides key elements to evaluate the structural controls on mineralization and constitutes the first kinematic data for the Carboniferous basement of the Southern Sierras Pampeanas. The polymetallic (Pb-Zn-Cu-Ag ± Au) vein systems of the Sierra de Comechingones were emplaced within NNW- and ENE-trending transtensional brittle-ductile shear zones that notably overprint the earlier metamorphic fabrics of the basement. Kinematic data indicate large components of strike-slip motion with subordinated normal-slip for the majority of the mineralized structures.

K/Ar age data from sericitic alteration reveal a Carboniferous hydrothermal event developed between ~329 and 315 Ma. These results yield a time difference of around 40 Ma between hydrothermal activity in the Las Guindas and Oro districts and the intrusion of the Late Devonian Cerro Áspero and Achala batholiths (Achalian magmatism), despite their close spatial proximity. The mineralization is rather temporally related to the emplacement of Early Carboniferous A-type granites of the Eastern Sierras Pampeanas (Early Gondwana magmatism).

In line with other regional evidence, we suggest a possible Carboniferous deformational phase, dominated by transtension. The polymetallic mineralization of the Sierra de Comechingones would have been emplaced close to the transition with the Devonian compressional/transpressional orogenic regime. This transtensional phase could play a significant role in the Sierras Pampeanas, controlling the emplacement of granitic plutons, hydrothermal ore veins, and sedimentation in the Paganzo basin.

Acknowledgments

This work is part of the PhD research of Dr. M.N. Maffini at the Universidad Nacional de Río Cuarto (UNRC), who was assisted by a scholarship from the Consejo Nacional de Investigaciones Científicas y Técnicas (CONICET). Investigations were financially supported by grants from the Agencia Nacional de Promoción Científica y Tecnológica (ANPCyT) and the Secretaría de Ciencia y Técnica, Universidad Nacional de Río Cuarto (SECyT-UNRC). The authors want to thank Lic. Nicolás Zambroni, M. Eugenia Muratori and M. Alejandra Boffadossi for field work and office assistance, and the Zabala family from Las Guindas farm for their hospitality and logistic facilities during field work. Dr. Roberto Miró is acknowledged for providing preliminary data of the Oro district and Dr. Milka de Brodtkorb for giving a constant scientific support. The authors also want to thank the editor of this journal as well as Roberto Weinberg and an anonymous reviewer for their comments and valuable corrections that contributed to significantly improve the quality of this manuscript.

References

Afifi, A.M., Kelly, W.C., Essene, E.J., 1988. Phase relations among tellurides, sulfides, and oxides; Pt. II, Applications to telluride-bearing ore deposits. Econ. Geol. 83 (2), 395–404. http://dx.doi.org/10.2113/gsecongeo.83.2.395.

Alasino, P.H., Dahlquist, J.A., Pankhurst, R.J., Galindo, C., Casquet, C., Rapela, C.W., Fanning, C.M., 2012. Early Carboniferous sub-to mid-alkaline magmatism in the Eastern Sierras Pampeanas, NW Argentina: a record of crustal growth by the incorporation of mantle-derived material in an extensional setting. Gondwana Res. 22 (3–4), 992–1008. http://dx.doi.org/10.1016/j.gr.2011.12.011.

Allmendinger, R.W., 2001. FaultKinWin, Version 1.1: a program for analyzing fault slip data for Windows™, http://www.geo.cornell.edu/geology/faculty/RWA/programs.html.

Allmendinger, R., Cardozo, N., Fisher, D., 2012. Structural Geology Algorithms: Vectors and Tensors. Cambridge University Press, Cambridge. http://dx.doi.org/10.1017/cbo9780511920202.

Angelier, J., 1984. Tectonic analysis of fault-slip data sets. J. Geophys. Res. 89 (B7), 5835–5848. http://dx.doi.org/10.1029/jb089ib07p05835.

Astini, R., Del Papa, C., 2014. Cubierta sedimentaria paleozoica superior. In: Martino, R.D., Guereschi, A.B. (Eds.), Geología y Recursos Naturales de la provincia de Córdoba. Asoc. Geol. Argent, Córdoba, pp. 393–419.

Astini, R.A., Martina, F., Ezpeleta, M., Dávila, F.M., Cawood, P.A., 2009. Chronology from rifting to foreland basin in the Paganzo Basin (Argentina), and a reapprisal on the "Eo-and Neohercynian" tectonics along Western Gondwana. In: Abstracts XII Congreso Geológico Chileno, Santiago S9–010 (Vol. 179).

Bense, F., Costa, C., Oriolo, S., Löbens, S., Dunkl, I., Wemmer, K., Siegesmund, S., 2017. Exhumation history and landscape evolution of the Sierra de San Luis (Sierras Pampeanas, Argentina) – new insights from low-temperature thermochronological data. Andean Geol. 44 (3). http://dx.doi.org/10.5027/andgeo%25x.

Biglia, M.E., Lira, R., Sfragulla, J.A., 2016. Nuevos datos mineralógicos, petrográficos y metalogenéticos del distrito minero Agua de Ramón, departamento Minas, Córdoba. Rev. Asoc. Geol. Argent. 73 (2), 225–241.

Boffadossi, M.A., Coniglio, J.E., Maffini, M.N., D'Eramo, F.J., Muratori, M.E., Demartis, M., 2016. Caracterización geológica-metalogenética de las mineralizaciones en stockwork vinculadas al magmatismo Devónico-Carbonífero de la Sierra de Comechingones, provincia de Córdoba. Acta Geol. Lilloana 28 (1), 40–44.

Clauer, N., 2013. The K-Ar and 40 Ar/39 Ar methods revisited for dating fine-grained K-bearing clay minerals. Chem. Geol. 354, 163–185. http://dx.doi.org/10.1016/j.chemgeo.2013.05.030.

Clauer, N., Chaudhuri, S., 1995. Clays in Crustal Environments. Isotope Dating and Tracing. Springer, Berlín Heidelberg, New York.
Collo, G., Astini, R.A., Cawood, P., Buchan, C., Pimentel, M., 2009. U-Pb detrital zircon ages and Sm-Nd isotopic features in low-grade metasedimentary rocks of the Famatina belt: implications for late Neoproterozoic-Early Paleozoic evolution of the proto-Andean margin of Gondwana. J. Geol. Soc. London 166 (2), 303–319. http://dx.doi.org/10.1144/0016-76492008-051.
Coniglio, J., 2006. Evolución petrológica y metalogenética del batolito Cerro Áspero en relación con el ciclo geoquímico endógeno del flúor, Sierra de Comechingones, Córdoba, Argentina. Unpublished PhD Thesis, Universidad Nacional de Río Cuarto, Río Cuarto, 163 pp.
Coniglio, J., Xavier, R.P., Pinotti, L., D'Eramo, F., 2000. Ore-forming fluids of vein-type fluorite deposits of the Cerro Aspero batholith, Southern Córdoba Province, Argentina. Int. Geol. Rev. 42 (4), 368–383. http://dx.doi.org/10.1080/00206810009465088.
Cox, D.P., Singer D.A., 1986. Mineral deposit models, First ed. U.S. Geol. Surv. Bull. Vol. 1693, Denver.
Dahlquist, J.A., Pankhurst, R.J., Rapela, C.W., Basei, M.A., Alasino, P.H., Saavedra, J., Baldo, E.G., Murra, J.A., Neto, M.D.C.C., 2016. The Capilla del Monte pluton, Sierras de Córdoba, Argentina: the easternmost Early Carboniferous magmatism in the pre-Andean SW Gondwana margin. Int. J. Earth Sci. 105 (5), 1287–1305. http://dx.doi.org/10.1007/s00531-015-1249-0.
Dahlquist, J.A., Alasino, P.H., Bello, C., 2014. Devonian F-rich peraluminous A-type magmatism in the proto-Andean foreland (Sierras Pampeanas, Argentina): geochemical constraints and petrogenesis from the western-central region of the Achala batholith. Miner. Petrol. 108 (3), 391–417. http://dx.doi.org/10.1007/s00710-013-0308-0.
Dahlquist, J.A., Pankhurst, R.J., Gaschnig, R.M., Rapela, C.W., Casquet, C., Alasino, P.H., Baldo, E.G., 2013. Hf and Nd isotopes in Early Ordovician to Early Carboniferous granites as monitors of crustal growth in the Proto-Andean margin of Gondwana. Gondwana Res. 23 (4), 1617–1630. http://dx.doi.org/10.1016/j.gr.2012.08.013.
Dahlquist, J.A., Alasino, P.H., Eby, G.N., Galindo, C., Casquet, C., 2010. Fault controlled Carboniferous A-type magmatism in the proto-Andean foreland (Sierras Pampeanas, Argentina): geochemical constraints and petrogenesis. Lithos 115 (1–4), 65–81. http://dx.doi.org/10.1016/j.lithos.2009.11.006.
de Brodtkorb, M., Conglio, J., Miró, R., 2014. Yacimientos Metalíferos y Metalogenia. In: Martino, R.D., Guereschi, A.B. (Eds.), Geología y Recursos Naturales de la provincia de Córdoba. Asoc. Geol. Argent, Córdoba, pp. 1025–1075.
Demartis, M., Pinotti, L.P., Coniglio, J.E., D'Eramo, F.J., Tubía Martínez, J.M., Aragón, E., Agulleiro Insúa, L.A., 2011. Ascent and emplacement of pegmatitic melts in a major reverse shear zone (Sierras de Córdoba, Argentina). J. Struct. Geol. 33 (9), 1334–1346. http://dx.doi.org/10.1016/j.jsg.2011.06.008.
Derez, T., Pennock, G., Drury, M., Sintubin, M., 2015. Low-temperature intracrystalline deformation microstructures in quartz. J. Struct. Geol. 71, 3–23. http://dx.doi.org/10.1016/j.jsg.2014.07.015.
Dewey, J.F., Holdsworth, R.E., Strachan, R.A., 1998. Transpression and transtension zones. Geol. Soc. Lond. Spec. Publ. 135 (1), 1–14. http://dx.doi.org/10.1144/gsl.sp.1998.135.01.01.
Dorais, M.J., Lira, R., Chen, Y., Tingey, D., 1997. Origin of biotite-apatite-rich enclaves, Achala batholith, Argentina. Contrib. Mineral. Petrol. 130 (1), 31–46. http://dx.doi.org/10.1007/s004100050347.
Drits, V.A., Weber, F., Salyn, A.L., Tsipursky, S.I., 1993. X-ray identification of one-layer illite varieties: application to the study of illites around uranium deposits of Canada. Clay Miner. 41 (3), 389–398. http://dx.doi.org/10.1346/ccmn.1993.0410316.
Enkelmann, E., Ridgway, K.D., Carignano, C., Linnemann, U., 2014. A thermochronometric view into an ancient landscape: tectonic setting, development, and inversion of the Paleozoic eastern Paganzo basin, Argentina. Lithosphere 6 (2), 93–107. http://dx.doi.org/10.1130/l309.1.
Fernandez-Seveso, F., Tankard, A.J., 1995. Tectonics and stratigraphy of the Late Paleozoic Paganzo Basin of Western Argentina and its regional implications. In: Tankard, A.J., Suárez Suroco, R., Welsink, H.J (Eds). Petroleum basins of South America, Memoir 62, pp. 285–301.
Fossen, H., Tikoff, B., 1998. Extended models of transpression and transtension, and application to tectonic settings. Geol. Soc. Lond. Spec. Publ. 135 (1), 15–33. http://dx.doi.org/10.1144/gsl.sp.1998.135.01.02.
Friedrich, D., 1991. Eine neue Methode zur Bestimmung der Illit-Kristallinität mit Hilfe digitaler Meßwerterfassung. Unpublished PhD Thesis, University of Göttingen, 63 pp.
Fuhrmann, U., Lippolt, H.J., Hess, J.C., 1987. Examination of some proposed K-Ar standards: 40Ar/39Ar analyses and conventional K-Ar-Data. Chem. Geol. (Isot. Geosci. Sect.). 66(1–2), pp. 41–51, doi: 10.1016/0168-9622(87)90027-3.
Gómez, G.M., 2003. El plutón de Serrezuela: Evento magmático del Carbonífero en el sector norte de la sierra de Pocho, Córdoba, República Argentina. Rev. Asoc. Geol. Argent. 58 (3), 283–297.
Guereschi, A., Martino, R., 2014. Las migmatitas de las Sierras de Córdoba. In: Martino, R.D., Guereschi, A.B. (Eds.), Geología y Recursos Naturales de la provincia de Córdoba. Asoc. Geol. Argent, Córdoba, pp. 67–94.
Guereschi, A.B., Martino, R.D., 2008. Field and textural evidence of two migmatization events in the Sierras de Córdoba, Argentina. Gondwana Res. 13 (2), 176–188. http://dx.doi.org/10.1016/j.gr.2007.07.005.
Haeberlin, Y., Moritz, R., Fontboté, L., 2003. Paleozoic orogenic gold deposits in the eastern Central Andes and its foreland, South America. Ore Geol. Rev. 22 (1–2), 41–59. http://dx.doi.org/10.1016/s0169-1368(02)00108-7.
Haines, S.H., van der Pluijm, B.A., 2008. Clay quantification and Ar–Ar dating of synthetic and natural gouge: application to the Miocene Sierra Mazatán detachment fault, Sonora, Mexico. J. Struct. Geol. 30 (4), 525–538. 10.1016/j.jsg.2007.11.012.
Harrison, T.M., Célérier, J., Aikman, A.B., Hermann, J., Heizler, M.T., 2009. Diffusion of 40 Ar in muscovite. Geochim. Cosmochim. Acta 73 (4), 1039–1051. http://dx.doi.org/10.1016/j.gca.2008.09.038.
Heinrichs, H., Herrmann, A.G., 1990. Praktikum der Analytischen Geochemie. Springer, Verlag Berlín Heidelberg.
Hongn, F., Ferreira, L., Morello, O., Rubinstein, N., Kirschbaum, A., Guidi, F., Anesa, J., 2010. Control estructural sobre el plutón Los Ratones y la mineralización de uranio en la sierra de Fiambalá, Sierras Pampeanas, Catamarca. Rev. Asoc. Geol. Argent. 67 (4), 545–561.
Hunziker, J.C., Frey, M., Clauer, N., Dallmeyer, R.D., Friedrichsen, H., Flehmig, W., Hochstrasser, K., Roggwiler, P., Schwander, H., 1986. The evolution of the illite to muscovite: mineralogical and isotopic data from the Glarus Alps, Switzerland. Contr. Mineral. Petrol. 92 (2), 157–180. http://dx.doi.org/10.1007/BF00375291.
Japas, M.S., Rubinstein, N.A., Gómez, A.L., 2015. Reverse Osmosis contributing to metal zoning in porphyry type deposits: a case study. Ore Geol. Rev. 71, 191–202. http://dx.doi.org/10.1016/j.oregeorev.2015.05.011.
Japas, M.S., Rubinstein, N.A., Kleiman, L.E., 2013. Strain fabric analysis applied to hydrothermal ore deposits emplaced during changing geodynamical conditions (Infiernillo and Las Picazas, San Rafael Massif, Argentina). Ore Geol. Rev. 53, 357–372. http://dx.doi.org/10.1016/j.oregeorev.2013.01.018.
Japas, M., Rubinstein, N., Morillo, O., 2004. Control estructural del Distrito minero Los Ratones, Sierra de Fiambalá, provincia de Catamarca. Avances en Microtectónica y Geología Estructural. Rev. Asoc. Geol. Argent, Serie D: Public. Esp. 7, 58–67.
Kelley, S., 2002. K-Ar and Ar-Ar dating. Rev. Mineral. Geochem. 47 (1), 785–818. http://dx.doi.org/10.2138/rmg.2002.47.17.
Kübler, B., 1967. La cristallinité de l'illite et les zones tout à fait supérieures de métamorphisme. In: Schaer, J.P. (Ed.), Colloque sur les étages tectoniques. À la Baconnière, Neuchâtel, pp. 105–122.
Limarino, C., Spalletti, L., 2006. Paleogeography of the upper Paleozoic basins of southern South America: an overview. J. S. Am. Earth Sci. 22 (3), 134–155.
Limarino, C., Tripaldi, A., Marenssi, S., Fauqué, L., 2006. Tectonic, sea-level, and climatic controls on Late Paleozoic sedimentation in the western basins of Argentina. J. S. Am. Earth Sci. 22 (3), 205–226.
Lira, R., Kirschbaum, A.M., 1990. Geochemical evolution of granites from the Achala batholith of the Sierras Pampeanas, Argentina. Geol. Soc. Am. Spec. Pap. 241, 67–76. http://dx.doi.org/10.1130/SPE241-p67.
Löbens, S., Oriolo, S., Benowitz, J., Wemmer, K., Layer, P., Siegesmund, S., 2016. Late Paleozoic deformation and exhumation in the Sierras Pampeanas (Argentina): 40Ar/39Ar-feldspar dating constraints. Int. J. Earth Sci. 1–13. http://dx.doi.org/10.1007/s00531-016-1403-3.
Löbens, S., Bense, F.A., Wemmer, K., Dunkl, I., Costa, C.H., Layer, P., Siegesmund, S., 2011. Exhumation and uplift of the Sierras Pampeanas: preliminary implications from K-Ar fault gouge dating and low-T thermochronology in the Sierra de Comechingones (Argentina). Int. J. Earth Sci. 100 (2–3), 671–694. http://dx.doi.org/10.1007/s00531-010-0608-0.
López de Luchi, M., Rapalini, A.E., Siegesmund, S., Steenken, A., 2004. Application of magnetic fabrics to the emplacement and tectonic history of Devonian granitoids in Central Argentina. Geol. Soc. Lond. Spec. Publ. 238 (1), 447–474. http://dx.doi.org/10.1144/gsl.sp.2004.238.01.23.
Lyons, P., Skirrow, R.G., Stuart-Smith, P.G., 1997. Informe Geológico y Metalogenético de Las Sierras Septentrionales de Córdoba, Provincia de Córdoba. 1:250.000. Unpublished reports to Serv. Geol. Min. Argent, Buenos Aires.
Macchioli Grande, M., Alasino, P.H., Rocher, S., Larrovere, M.A., Dahlquist, J.A., 2015. Asymmetric textural and structural patterns of a granitic body emplaced at shallow levels: the La Chinchilla pluton, northwestern Argentina. J. S. Am. Earth Sci. 64 (1), 58–68. http://dx.doi.org/10.1016/j.jsames.2015.09.011.
Maffini, M.N., 2015. Estudio petro-estructural, mineralógico y metalogenético de depósitos vetiformes mesotermales (Pb-Zn-Cu-Ag-Au) emplazados en el basamento metamórfico de la Sierra de Comechingones, en proximidad a cuerpos ígneos plutónicos, Sierras Pampeanas Orientales. Unpublished PhD Thesis, Universidad Nacional de Río Cuarto, Río Cuarto, 284 pp.
Maffini, M.N., Ducart, D.F., Radice, S., Coniglio, J., D'Eramo, F., Demartis, M., Pinotti, L., Moreira Silva, A., Bemfica Toledo, C.L., 2017. Estudio petrográfico, espectral y de susceptibilidad magnética de la alteración hidrotermal asociada con depósitos polimetálicos de Pb-Zn-Cu-Ag-Au, Sierra de Comechingones, Córdoba (Argentina). Estud. Geol. 73 (1), e061. http://dx.doi.org/10.3989/egeol.42408.403.
Maffini, M.N., Coniglio, J.E., Demartis, M., D'Eramo, F.J., Pinotti, L.P., Bin, I., y Petrelli, H.A., 2012. Vetas mesotermales de Pb-Zn-Ag-Au emplazadas al este del Batolito Cerro Áspero, Sierra de Comechingones, Córdoba. Serie de Correlación Geológica 28 (2), 93–106.
Marrett, R., Allmendinger, R.W., 1990. Kinematic analysis of fault-slip data. J. Struct. Geol. 12 (8), 973–986. http://dx.doi.org/10.1016/0191-8141(90)90093-e.
Martino, R., 2003. Las fajas de deformación dúctil de las Sierras Pampeanas de Córdoba: una reseña general. Rev. Asoc. Geol. Argent. 58 (4), 549–571.
Miró, R.C., 1999. Los depósitos auríferos de Candelaria y San Ignacio, Córdoba. In: Zappettini, E.O. (Ed.), Recursos Minerales de la República Argentina. Instituto de Geología y Recursos Minerales, Buenos Aires, pp. 647–653.

Miró, R., Candiani J.C., 1985. Informe técnico minero. Dirección Nacional de Minería y Geología. Unpublished reports to Serv. Geol. Min. Argent., Buenos Aires.
Morales Cámera, M.M., Dahlquist, J.A., Basei, M.A., Galindo, C., Neto, M.D.C.C., Facetti, N., 2016. F-rich strongly peraluminous A-type magmatism in the pre-Andean foreland Sierras Pampeanas, Argentina: Geochemical, geochronological, isotopic constraints and petrogenesis. Lithos, 210–227. doi: 10.1016/j.lithos.2016.10.035.
Moore, D.M., Reynolds, R.C., 1997. X-ray Diffraction and the Identification and Analysis of Clay Minerals. Oxford University Press, New York.
Mutti, D., González Chiozza, S., 2005. Evolución petrotectónica del distrito minero Cerro Áspero y modelo de emplazamiento de los depósitos wolframíferos, Córdoba. Rev. Asoc. Geol. Argent. 60 (1), 159–173.
Mutti, D., Di Marco, A., Geuna, S., 2007. Depósitos polimetálicos en el orógeno famatiniano de las Sierras Pampeanas de San Luis y Córdoba: fluidos, fuentes y modelos de emplazamiento. Rev. Asoc. Geol. Argent. 62 (1), 44–61.
Mutti, D., Tourn, S., Caccaglio, O., Herrmann, C., Geuna, S., Di Marco, A., González Chiozza, S., 2005. Evolución metalogenética de las Sierras Pampeanas de Córdoba y sur de Santiago del Estero: Ciclos Famatiniano, Gondwánico y Ándico. Rev. Asoc. Geol. Argent. 60 (3), 467–485.
Otamendi, J., Castellarini, P., Fagiano, M., Demichelis, A., Tibaldi, A., 2004. Cambrian to Devonian geologic evolution of the Sierra de Comechingones, Estern Sierras Pampeanas, Argentina: evidence for the development and exhumation of continental crust on the proto-pacific margin of Gondwana. Gondwana Res. 7 (4), 1143–1155. http://dx.doi.org/10.1016/s1342-937x(05)71090-x.
Peacor, D.R., Bauluz, B., Dong, H., Tillick, D., Yan, Y., 2002. Transmission and analytical electron microscopy evidence for high Mg contents of 1M illite: absence of 1M polytypism in normal prograde diagenetic sequences of pelitic rocks. Clay. Clay Miner. 50 (6), 757–765. http://dx.doi.org/10.1346/000986002762090281.
Pinotti, L., Tubía, J.M., D'Eramo, F., Vegas, N., Sato, A.M., Coniglio, J., Aranguren, A., 2006. Structural interplay between plutons during the construction of a batholith (Cerro Áspero batholith, Sierras de Córdoba, Argentina). J. Struct. Geol. 28 (5), 834–849. http://dx.doi.org/10.1016/j.jsg.2006.02.004.
Pinotti, L.P., Coniglio, J.E., Esparza, A.M., D'Eramo, F.J., Llambías, E.J., 2002. Nearly circular plutons emplaced by stoping at shallow crustal levels, Cerro Áspero batholith, Sierras Pampeanas de Córdoba, Argentina. J. S. Am. Earth Sci. 15 (2), 251–265. http://dx.doi.org/10.1016/s0895-9811(02)00033-0.
Purdy, J.W., Jäger, E., 1976. K-Ar ages on rock-forming minerals from the Central Alps. Mem. Ist. Geol. e Min., Univ. Padova 30, 1–31.
Radice, S., Pinotti, L. Lince Klinger, F., Giménez, M., Fagiano, M., D'Eramo, F., Nacif, S., Zambroni, N., Demartis, M., 2015. Evidencias geofísicas de cuerpo ígneos no aflorantes en la porción centro-norte de la Sierra de Comechingones, Córdoba, Argentina. In: Abstracts 3° Simposio sobre Petrología Ígnea y Metalogénesis Asociada, Río Negro, Argentina, 136–137.
Ramos, V., 1988. Tectonics of the Late Proterozoic-Early Paleozoic: a collisional history of Southern South America. Episodes 11 (3), 168–174.
Ramsay, J.G., Huber, M.I., 1987. The Techniques of Modern Structural Geology: Fold and Fractures, vol. 2. Academic Press, London. first ed..
Rapela, C., Baldo, E., Pankhurst, R., Fanning, C., 2008. The Devonian Achala Batholith of the Sierras Pampeanas: F-rich, aluminous A-types granites. In: VI South American Symposium on Isotope Geology, San Carlos de Bariloche, Argentina. Proceedings in CD-ROM, paper 53.
Rapela, C.W., Pankhurst, R.J., Casquet, C., Fanning, C.M., Baldo, E.G., González Casado, J.M., Dahlquist, J., 2007. The Río de la Plata craton and the assembly of SW Gondwana. Earth Sci. 83 (1–2), 49–82. http://dx.doi.org/10.1016/j.earscirev.2007.03.004.
Rapela, C., Casquet, C., Baldo, E., Dahlquist, J., Pankhurst, R.J., Galindo, C., Saavedra, J., 2001. Las orogénesis del Paleozoico Inferior en el margen proto-andino de América del Sur, Sierras Pampeanas, Argentina. J. Iber. Geol. 27, 23–41.
Rapela, C., Pankhurst, R., Casquet, C., Baldo, E., Saavedra, J., Galindo, C. y Fanning, C., 1998. The Pampean orogeny of the southern proto-Andes: Cambrian continental collision in the Sierras de Córdoba. In Pankhurst, R., Rapela, C. (Eds.), The Proto-Andean margin of Gondwana. Geol. Soc. Lond. Spec. Publ. 142 (1), pp. 181–217, doi: 10.1144/gsl.sp.1998.142.01.10.
Sanderson, D.J., Marchini, W.R.D., 1984. Transpression. J. Struct. Geol. 6 (5), 449–458. http://dx.doi.org/10.1016/0191-8141(84)90058-0.
Schumacher, E., 1975. Herstellung von 99,9997% ^{38}Ar für die $^{40}K/^{40}Ar$ Geochronologie. Geochron. Chimia. 24, 441–442.
Siegesmund, S., Steenken, A., Martino, R.D., Wemmer, K., De Luchi, M.G.L., Frei, R., Guereschi, A., 2010. Time constraints on the tectonic evolution of the Eastern Sierras Pampeanas (Central Argentina). Int. J. Earth Sci. 99 (6), 1199–1226. http://dx.doi.org/10.1007/s00531-009-0471-z.
Siegesmund, S., Steenken, A., De Luchi, M.L., Wemmer, K., Hoffmann, A., Mosch, S., 2004. The Las Chacras-Potrerillos batholith (Pampean Ranges, Argentina): structural evidences, emplacement and timing of the intrusion. Int. J. Earth Sci. 93 (1), 23–43. http://dx.doi.org/10.1007/s00531-003-0363-6.
Sims, J., Ireland, T., Camacho, A., Lions, P., Pieters, P., Skirrow, R., Stuart Smith, P., Miró, R., 1998. U-Pb, Th-Pb and Ar-Ar geochronology from the southern Sierras Pampeanas, Argentina: implications for the Paleozoic tectonic evolution of the western Gondwana margin. Geol. Soc. Lond. Spec. Publ. 142 (1), 259–281. http://dx.doi.org/10.1144/gsl.sp.1998.142.01.13.
Skirrow, R.G., Camacho, A., Lyons, P., Pieters, P.E., Sims, J.P., Stuart Smith, P.G., Miró, R., 2000. Metallogeny of the southern Sierras Pampeanas, Argentina: Geological, 40Ar-39Ar dating and stable isotope evidence for Devonian Au, Ag-Pb-Zn and W or formation. Ore Geol. Rev. 17 (1–2), 39–81. http://dx.doi.org/10.1016/s0169-1368(00)00004-4.
Steenken, A., Wemmer, K., Martino, R.D., López de Luchi, M.G., Guereschi, A., Siegesmund, S., 2010. Post-Pampean cooling and the uplift of the Sierras Pampeanas in the west of Córdoba (Central Argentina). N. Jb. Geol. Paläont. 256 (2), 235–255. http://dx.doi.org/10.1127/0077-7749/2010/0094.
Steiger, R.H., Jäger, E., 1977. Subcommission on geochronology: convention on the use of decay constants in geo- and cosmochronology. Earth Planet. Sci. Lett. 36 (3), 359–362. http://dx.doi.org/10.1016/0012-821x(77)90060-7.
Stuart Smith, P.G., Camacho, A., Sims, J.P., Skirrow, R.G., Lyons, P., Pieters, P.E., Black, L.P., Miró, R., 1999. Uranium-lead dating of felsic magmatic cycles in the southern Sierras Pampeanas, Argentina: implications for the tectonic development of the proto-Andean Gondwana margin. Geol. Soc. Am. Spec. Pap. 336, 87–114. http://dx.doi.org/10.1130/0-8137-2336-1.87.
Sureda, R., 1978. Las vetas de plomo, plata y zinc del distrito minero El Guaico en la provincial de Córdoba, República Argentina. Rev. Asoc. Geol. Argent. 33 (4), 299–324.
Thomas, W., Astini, R., 2003. Ordovician accretion of the Argentine Precordillera terrane to Gondwana. J. S. Am. Earth Sci. 16 (1), 67–79. http://dx.doi.org/10.1016/s0895-9811(03)00019-1.
Ulacco, J.H., 2001. Magmatism and mineralization ages from northeast area of La Sierra de San Luis, Argentina. In: extended abstracts 3° South American symposium on isotope geology, Pucon, Chile, 535–538.
Ulacco, J.H., Ortíz Suarez, A., Ramos, G.A., 2005. Las minas Piedras Bayas y La Sala, Provincia de San Luis, criaderos de Pb, Zn y V. Serie de Correlación Geológica 19, 113–122.
Velde, B., 1965a. Experimental determination of muscovite polymorph stabilities. Am. Mineral. 50, 436–449.
Velde, B., 1965b. Phengite micas: synthesis, stability, and natural occurrence. Am. J. Sci. 263 (10), 886–913. http://dx.doi.org/10.2475/ajs.263.10.886.
Verdel, C., Niemi, N., Van Der Pluijm, B.A., 2011. Variations in the illite to muscovite transition related to metamorphic conditions and detrital muscovite content: insight from the paleozoic passive margin of the Southwestern United States. J. Geol. 119 (1), 419–437. http://dx.doi.org/10.1086/660086.
Villa, I.M., 1998. Isotopic closure. Terra Nova 10 (1), 42–47. http://dx.doi.org/10.1046/j.1365-3121.1998.00156.x.
Wemmer, K., 1991. K/Ar-Altersdatierungsmöglichkeiten für retrograde Deformationsprozesse im spröden und duktilen Bereich – Beispiele aus der KTB-Vorbohrung (Oberpfalz) und dem Bereich der Insubrischen Linie (N-Italien). Göttinger Arbeiten zur Geologie und Paläontologie 51, 1–61.
Wemmer, K., Ahrendt, H., 1997. Comparative K-Ar and Rb-Sr age determinations of retrograde processes on rocks from the KTB deep drilling project. Geol. Rundsch. 86 (S1), S272–S285. http://dx.doi.org/10.1007/pl00014660.
Wemmer, K., Steenken, A., Müller, S., de Luchi, M.G.L., Siegesmund, S., 2011. The tectonic significance of K/Ar illite fine-fraction ages from the San Luis Formation (Eastern Sierras Pampeanas, Argentina). Int. J. Earth Sci. 100 (2–3), 659–669. http://dx.doi.org/10.1007/s00531-010-0629-8.
Whitmeyer, S., 2008. Dating fault fabrics using modern techniques of 40 Ar/39 Ar thermochronology: evidence for Paleozoic deformation in the Eastern Sierras Pampeanas, Argentina. J. Virtual Explorer, Electronic Edition, Vol. 30, paper 3. http://csmres.jmu.edu/Geollab/Whitmeyer/web/documents/Whitmeyer%202008.pdf DOI: 10.3809/jvirtex.2008.00207.